DETERMINATION OF CONVECTIVE HEAT TRANSFER COEFFICIENTS FROM BOUNDARY LAYER PROFILES AND APPLICATION TO SURFACE ROUGHNESS

by

Lawrie Ray Nichol

A Thesis Presented in Partial Fulfillment
of the Requirements for the Degree
Master of Science

The Faculty of Graduate Studies
Department of Mechanical Engineering
University of Manitoba

August 1963

ABSTRACT

The work described herein is an attempt to adapt hydrodynamic and thermal boundary layer theory for annular flow as applied to rough surfaces. The theory was tested experimentally on four tubes over a limited Reynolds number range.

Convective heat transfer coefficients have been generally obtained by heat balances and correlated by dimensionless parameters obtained by dimensional analysis and modified semi-empirically. Few researchers have used the available boundary layer theories to calculate the heat transfer coefficients. However, the literature indicates there is a relationship between the surface roughness and the boundary layer thicknesses. The boundary layer profiles therefore were used to determine the heat transfer coefficients because this procedure gives a better insight into the effects of surface roughness. The availability of equipment and preliminary attempts to produce a rough surface led to the use of an annular type of test configuration.

In preparation for the development of the theory a derivation of Reynolds' analogy is shown followed by resumés of some of the published data which are appropriate to this work. The theory for hydrodynamic and thermal boundary layer is then developed for annular flow from flat plate theory.

A description of the apparatus and the experimental procedure are included and, in concluding, the experimental results are compared to the theory of others.

ACKNOWLEDGEMENTS

The author is indebted to Professor R. E. Chant for his assistance and guidance, to the National Research Council of Canada who provided financial aid in the form of a Studentship, to the technicians who assisted in fabricating the equipment and to all others associated with the project.

GLOSSARY OF TERMS

ALPHABETICAL SYMBOLS

A = surface area of the test section – ft^2.

C = specific heat – Btu/lb°F.

De = equivalent diameter=D_2-D_1–ft.

E = total energy Btu or ft–lbs.

EH = eddy diffusivity of heat – ft^2/sec.

EM = eddy diffusivity of momentum – ft^2/sec.

e = arithmetic mean surface roughness – micro–ins./inch.

f = Fanning friction factor = $g \frac{2\Delta p \rho}{G^2} \frac{De}{L} \frac{D_1}{D_2}$

g = local acceleration of gravity, 32.2 ft/sec.^{2}

G = weight flow - lbs/hr.ft.^{2} or lbs/sec.ft.^{2}

h = convective heat transfer coefficient Btu/hr.ft.^{2}°F

j = $\frac{h}{C_{\rho b} G} \left(\frac{C p \mu}{k}\right)^{2/3}$.

j^1 = $j \left(\frac{\mu w}{\mu b}\right)^{0.14}$.

k = thermal conductivity – Btu/hr.ft.°F

K = (NST/F/2)/(NST_o/F_o/2).

L = length from leading edge of test specimen–ft.

p = pressure – lbs/ft.^{2}

Q = total heat flow – Btu/hr.

r = radius – ft.

q = Heat transfer – Btus/hr.

t = temp. °F

u = velocity ft/sec.

V = volume $ft.^3$

W = work Btu/lb.

y = $r - r_1$ — ft.

GREEK LETTERS

α = diameter ratio $= D_1/D_2$.

Δ = hydrodynamic boundary layer thickness — ft.

Δ_t = thermal boundary layer thickness — ft.

Δ_3 = kinetic energy thickness $= \int_o^{\Delta} \frac{u}{u_\Delta}\left(1-\left(\frac{u}{u_\Delta}\right)^2\right)\frac{\rho}{\rho_\Delta}\frac{rdr}{r_w}$ *.

Δ_{t_2} = enthalpy thickness $= \int_o^{\Delta} \frac{u}{u_\Delta}\left(\frac{t-t_\Delta}{t_w-t_\Delta}\right)\frac{\rho}{\rho_\Delta}\frac{r}{r_w}dr$ *.

λ = r_m/r_2.

Θ = time.

μ = dynamic viscosity — lbs/hr. ft or lbs/sec.ft.

Φ = flux density — Btu/hr.$ft.^2$

ρ = density — lbs/cu.ft.

γ = shear stress $= \mu\frac{du}{dy}$ — lbs/$ft.^2$

DIMENSIONLESS NUMBERS

NRE = Reynolds Number $= \left(\frac{DeU\rho}{\mu}\right)_b$

* For flow in an annulus.

NNU = Nusselt Number = $(\frac{hDe}{k})_b$

NST = Stanton Number = $(\frac{h}{CpU\rho})_b$

NPR = Prandtl Number = $(\frac{Cp\mu}{k})_b$

SUBSCRIPTS

1 = at inner wall of annulus

2 = at outer wall of annulus

a = value calculated from formulae

m = point of max. velocity

M = mean

b = at bulk conditions

o = temperature of flow if no heat addition

p = at constant pressure

v = at constant volume

w = at inner wall of annulus

δ = at outer extremity of the boundary layer.

TABLE OF CONTENTS

LIST OF TABLES

LIST OF FIGURES

CHAPTER 1

INTRODUCTION

The work described herein is an attempt to develop hydrodynamic and thermal boundary layer theory for annular flow as applied to rough surfaces. It was tested experimentally on four tubes over a limited Reynolds number range.

Convective heat transfer coefficients have been generally obtained by heat balances and correlated by dimensionless parameters arrived at by dimensional analysis and modified semi-empirically. Few researchers have used the available boundary layer theories to calculate the heat transfer coefficients . However, the literature indicates there is a relationship between the surface roughness and the boundary layer thickness. The boundary layer profiles therefore were used to determine the heat transfer coefficients because the procedure should give a better understanding of the effects of surface roughness.

Until recently most of the studies of the effect of surface roughness on convective heat transfer have been restricted to the inside of pipes, rectangular ducts and flat plates. Some of the workers in this field have been Durant and Mirshak (7)*, Lancet (12), Levy and Sebane (13), Nunner (18) and Smith and Epstein (17). Their work varied from the very

* Numbers in italics refer to references in Bibliography.

theoretical to the quite practical and many advances have been made towards a complete knowledge of the effects of surface roughness in particular flow configurations. The availability of the equipment and preliminary attempts to produce a rough surface led to the use of an annular type of test configuration.

In preparation for the development of the theory a derivation of Reynolds' analogy is shown, followed by resumes of some of the printed literature which is appropriate to this work. This includes work by such authors as McAdam (14), Kemeny and Cyphers (10), Barrow (1), Patterson and Durands (16), Knudsen (11) and Brunello (3). The theory for hydrodynamics and thermal boundary layers was then developed for annular flow from the flat plate theory advanced by Brunello

A description of the apparatus and the experimental procedure are included and, in concluding, the experimental results are compared to the theory of others.

CHAPTER 2

BASIC PRINCIPLES AND PUELISHED DATA

The convective heat transfer coefficient is a parameter used to determine the amount of heat flow from a surface to a fluid and is analogous to replacing the thermal conductivity (k) in the equation

$$Q = -kA\frac{dt}{dx}$$

Since the amount of heat transferred to or from a fluid is determined by the hydrodynamic boundary layer the convective heat transfer coefficient is dependent on this boundary layer.

The roughening of a heat transfer surface has a three-fold result. The roughness increases the surface area of the element, creates turbulence which transfers heat into the high velocity main stream, and increases the friction factor.

When the entire wetted perimeter is roughened the friction factor has been found to increase faster than the convective heat transfer coefficients so the advantages of surface roughness are either reduced or vitiated, depending on local power costs.

The following is an analysis of Reynolds' analogy and a discussion of the published material containing methods related to this analogy. This is done by first determining a semi-empirical equation which predicts the friction factor and then by Reynolds' analogy a formula for the heat transfer coefficient is obtained.

2-1 BASIC PRINCIPLES

In turbulent flow three forms of heat transfer are present. In the neighbourhood of the heat transfer surface the fluid is essentially at rest and conduction is the only method by which heat is transferred. As the distance from the surface is increased the amount of heat transported by the high velocity core increases until convection becomes the dominant mode. In turbulent flow the third mode is caused by a continuous mixing of the fluid particles due to the velocity fluctuations. While the mechanism of this mass transfer is fairly well understood, mathematical analyses are impractical for engineering purposes.

Since the velocities near the surface are nearly at rest heat can be considered to move perpendicular to the surface in the case of a flat plate, or radially, in the case of a circular section. Prandtl considered the layer adjacent to the wall to be laminar and that no heat was transferred by turbulent mixing in this layer. Outside this layer Prandtl considers conduction and shear small enough to be neglected. With conduction and shear neglected the heat in the turbulent core is transferred by macroscopic mass movement, eddy diffusion. The entire process is covered by the term convection. The case analysed below and of concern in this thesis is forced convection which is the term used to describe the

process when there is an affected flow of the fluid over the surface.

The eddy diffusion of momentum (EM) is described by the equation:

$$\tau = (\mu + \rho EM) \frac{du}{dy} \quad \ldots\ldots\ldots\ldots\ldots\ldots \quad 2.1$$

In the laminar sublayer EM reduces to zero leaving the formula for viscous shear

$$\tau_w = \mu \frac{du}{dy}$$

The eddy diffusion of heat (EH) is described by a similar equation

$$\frac{q}{A} = -(k + \rho C_p EH) \frac{dt}{dy} \quad \ldots\ldots\ldots\ldots\ldots\ldots \quad 2.2$$

In the laminar sublayer the eddy diffusivity becomes zero leaving the formula for pure conduction

$$\frac{q}{A} = -k \frac{dt}{dy}$$

2.2 REYNOLDS' ANALOGY

If the flow in an annulus is well enough developed to neglect the effects of the outside wall on the inner boundary

layer and the radial pressure gradient is neglected the relation $\tau/\tau_w = r/r_w$ exists for local shear stress. Assuming that a similar condition exists for heat flux:

$$\frac{q/A}{(q/A)_w} = \frac{r}{r_w}$$

Equation 2.1 and 2.2 can now be written:

$$\frac{q_w}{A_w \rho C_p}\left(1 + \frac{y}{r_w}\right) = -\left(\frac{k}{C_p \rho} + EH\right)\frac{dt}{dy} \qquad \text{..... 2.3}$$

$$\frac{\tau_w}{\rho}\left(1 + \frac{y}{r_w}\right) = \left(\frac{\mu}{\rho} + EM\right)\frac{du}{dy} \qquad \text{..... 2.4}$$

The term $(k/\rho C_p + E_H)$ is considered as a turbulent Prandtl number and the term $(\frac{\mu}{\rho} + E_M)$ as a turbulent kinematic viscosity. If the terms are equal, equation 2.5 results from dividing 2.3 by 2.4. This implies E_H has the same effect on the heat transfer as E_M has on the shear force, also $\rho\frac{k}{C_p} = \frac{\mu}{\rho}$ means $\frac{k}{\mu C_p} = 1$ or NPR = 1 which restricts its applications to fluids with NPR's from 0.7 to 2.0.

$$\frac{q_w\, du}{A_w C_p\, \tau_w} = -dt \qquad \text{..... 2.5}$$

Integrating u from 0 to U_s and t from t_w to t_b and substituting in the definitions,
$h = q_w/A_w(t_w - t_b)$ and $\tau_w = f\rho U^2/2$

Reynolds' analogy is obtained.

$$NST = \frac{h}{\rho C_p U} = \frac{f}{2} \qquad \text{..... 2.6}$$

This formula was first developed in 1874 by Osborne Reynolds; from equation 2.5 it can also be written in terms of the heat flux as follows:

$$\Phi = \frac{q_w}{A_w} = -\tau_t \, c_p \frac{dt}{du} \qquad \ldots\ldots\ldots\ldots\ldots\ldots\ldots\ldots \quad 2.7$$

The derivation of Reynolds' analogy implies a Prandtl number (NPR = $\frac{\mu c_p}{k}$) of unity and equal thermal and momentum diffusivities. However, the analogy is assumed to apply for Prandtl numbers ranging from 0.70 to 2.0 or higher and serves as a first approximation for most convective heat transfer analysis. More advanced theoretical analyses yield a complex function of the NPR when relating the NST to the f/2 which in practice is often replaced by $NPR^{2/3}$. That is:

$$NST \; NPR^{2/3} = \frac{f}{2} = \text{Colburn Equation (14)} \qquad \ldots\ldots\ldots\ldots\ldots \quad 2.8$$

With Reynolds' analogy assumed to apply for air (NPR = 0.7) semi-empirical equations that have been obtained by other authors can be used as a comparison in this work. If the viscosity changes appreciably with temperature an additional correction factor is necessary but for the work described herein it has been neglected.

Although heat transfer and friction effects in an annulus have not been studied extensively some authors have

advanced formulas corrected to annular flow from flat plate or duct experiments.

2-3 RECENT THEORIES ON ANNULAR HEAT TRANSFER

Knudsen J.G. (11)

The author analysed the velocity profile unique to annular flow and the derivation is shown below.

Taking a force balance on an element of steady fully developed turbulent flow the shear stresses can be related as follows:

$$\frac{\tau_1}{\tau_2} = \frac{r_2}{r_1}\,\frac{(r_m^2 - r_1^2)}{(r_2^2 - r_m^2)} = \frac{\lambda^2 - \alpha^2}{\alpha(1-\lambda^2)} \qquad \text{..... 2.9}$$

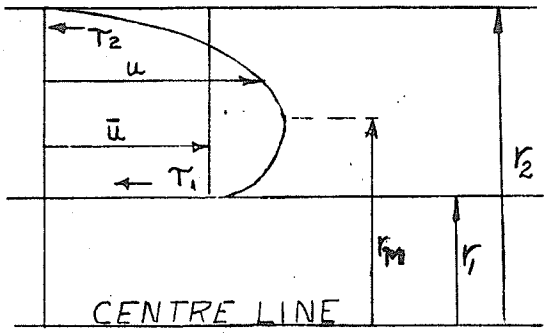

Where:

$$r_m^2 = \frac{r_2^2 - r_1^2}{\ln\left[\frac{r_1}{r_2}\right]^2} \qquad \text{..... 2.10}$$

or $$\lambda^2 = \frac{1-\alpha^2}{\ln \alpha^2}$$

Dealing exclusively with the inside wall the friction factor can be defined as:

$$f_1 = \frac{\tau_1 / \rho \; u^2}{2g_c} \qquad \text{..... 2.11}$$

But $$\frac{f_1}{f_2} = \frac{\tau_1}{\tau_2} = \frac{\lambda^2 - \alpha^2}{\alpha(1-\lambda^2)} \qquad \text{..... 2.12}$$

For turbulent flow inside a tube

$$f = .046\ (NRE)^{-0.2} \qquad \ldots\ldots\ldots\ldots\ldots\ldots\ 2.13$$

That is $\frac{f_2}{2} = .023\ (NRE)_2^{-0.2}$ $\qquad \ldots\ldots\ldots\ldots\ldots\ldots\ 2.14$

where $(NRE)_2 = \frac{U_2 D_2 \rho}{\mu}$

The flow is considered to be divided into two regimes from $D = D_2$ to $D = D_m$ and from $D = D_1$ to $D = D_m$ where U_2 is a fictitious velocity assumed to be applicable at the outer surface and for continuity of flow,

$$U_2 D_2^{\,2} = \bar{u}\ (D_2^{\,2} - D_m^{\,2})$$

whence $$U_2/\bar{u} = (D_2^{\,2} - D_m^{\,2})/D_2^{\,2} = 1 - \lambda^2$$

Then $$(NRE)_2 = \frac{\rho \bar{u} D_e}{\mu} \times \frac{1 - \lambda^2}{1 - \alpha}$$

and $$\frac{f_2}{2} = .023 (NRE)_b^{-0.2} \times \left(\frac{1 - \alpha}{1 - \lambda^2}\right)^{0.2} \qquad \ldots\ldots\ldots\ldots\ 2.15$$

From 2.11

$$j = \frac{f_1}{2} = .023 (NRE)_b^{-0.2} \times \left(\frac{1 - \alpha}{1 - \lambda^2}\right)^{0.2} \qquad \ldots\ldots\ldots\ldots\ 2.16$$

which is applicable for heat transfer from the inner cylinder of an annulus for NRE from 1×10^4 to 1×10^5.

For the radius ratio used in the experiments described herein $r_2/r_1 = 2.69$ and the expression 2.16 becomes

$$j = 0.035\ NRE^{-0.2} \qquad \ldots\ldots\ldots\ldots\ 2.17$$

W.H. McAdams (14).

In the calculation of the average heat transfer coefficient for an annulus McAdams suggests that the following formula be used:

$$j = NST\ NPR^{2/3} = 0.023\ NRE^{-0.2} \quad \ldots\ldots\ldots\ldots\ldots\ldots\ 2.18$$

The above formula is recommended for convective coefficients on the inside of tubes.

To adapt the following equation Weigand multiplied the right hand side by a ratio of $\left(\frac{D_2}{D_1}\right)^{0.45}$.

Similar factors consisting of diameter ratios have been developed by other authors and are listed in the references. The development of such a ratio is shown under Knudsen's work.

Kemeny, C.A. and Cyphere, J.A. (10)

These authors did some extensive work on the pressure drop in an annular configuration caused by surface spoilers and derived an equation based on theory previously advanced in Carslaw and Jaeger, and from formulas developed by Nunner.

$$f = NRE^{.05} \left(\frac{H}{De}\right) \left[0.593 - 0.208 \left(\ln \frac{10H}{P}\right)^{8/5}\right] \ldots\ldots\ 2.19$$

This work is one of the few published on heat transfer

and friction in an annulus using surface spoilers but has not as yet been verified by other investigators. A formula for use in calculating the heat transfer coefficient on the inside pipe was not advanced. They compared the ratios of 2j/f versus NRE as a criterion upon which the various tubes could be evaluated. They also use a ratio of $j/f\rho u$ but the advantages of using such a ratio are not apparent because the scope of the work is limited.

The authors advance a formula for calculating the friction factor and, if Reynolds' analogy is assumed to hold an equation for the Nusselt (NNU) or NST is obtained. This equation is as follows:

$$(NPR)^{2/3}\ NST = \frac{1}{2} NRE^{0.05} \left(\frac{H}{D_e}\right) \left[0.593-0.208 \left(\ln \frac{10H}{P}\right)^{8/5}\right] \ldots\ 2.20$$

or changed to NNU by the relationship

$$NST = \frac{NNU}{NRE\ NPR}$$

Barrow, H. (1)

Starting with the concept of momentum and thermal diffusivity and considering a region where turbulent mixing predominates he applies Reynolds' analogy again implying the two diffusivities are equal. In order to account for the type

of velocity profile inherent in annular flow, he obtains an equation for a fictitious radius (r_f) slightly larger than the inside pipe so that the shear stress at this fictitious radius (γw_f) equals the shear stress at the outside wall (γw_2). This brings his results into agreement with the literature cited.

The final formula advanced by Barrow is:

$$NNU = 0.0346\ NRE^{3/4}\ F_1F_3/F_2 \quad \ldots\ldots\ldots\ldots\ldots\ldots\ 2.21$$

Where

$$\alpha = \frac{r_2}{r_1}$$

$$F_1 = \frac{\gamma w_1}{\gamma w_2} = \alpha\left[\frac{\alpha^2-1-2\ln\alpha}{2\alpha^2\ln\alpha-\alpha^2+1}\right]$$

$$F_2 = 1 + q_m/q_w \qquad q_m = \text{heat flow at max.vel.}$$

$$F_3 = \left[\frac{NRE\ 2}{NRE_b}\right]^{-1/4}$$

$$r_f = \frac{r_m^2}{r_2}$$

The equivalent diameter is described as:

$$de_2 = 2\left(\frac{r_2^2 - r_m^2}{r_2}\right)$$

$$NRE_2 = 2(r_2^2-r_m^2)\ \bar{u}\rho/\ r_2\mu$$

This theory is applied with a friction factor derived from the shear forces on the wall. The velocity distributions for this work are taken as a modified 1/7 power law which described the velocity profiles from both the outside and inside walls relative to the maximum velocity. The friction factor used is $f = 0.079\ NRE^{-0.25}$, which when combined with Reynolds' analogy yields equation 2.21.

Of the formulas presented in this chapter those of Knudsen, Barrow, McAdams and Weigand were chosen to be used as a comparison with this work. Barrows and McAdams approximate one another over a much larger Reynolds number range than those encountered in this work which was $.8 \times 10^5$ to 1.4×10^5. The Knudsen and Weigand formulas are close but not such a close approximation to one another as Barrow and McAdams. The Knudsen and Weigand formulas are also much higher than the other two when the Nusselt number versus Reynolds number is graphed.

CHAPTER 3

HYDRODYNAMIC AND THERMAL BOUNDARY LAYER THEORY

With the exception of section 2.7 the last chapter is devoted to showing the equations and methods put forward by various authors to enable the overall heat transfer coefficient to be calculated. All this work depended on the accurate metering of power input with no other way of determining their results.

Attempts have been made to analyse the flow in annuli. One of these attempts is given in reference 2. This work develops from Navier - Stokes equation in cylindrical co-ordinates. The final result is an equation for the flow (G) as a function of the inside and outside radii, pressure drop and dynamic viscosity. However, one of the few methods which include both a thermal and hydrodynamic analysis is the method initiated by Brunello.

Although Brunello's work does not apply to annular flow it is described here since the method by which the heat transfer coefficients have been calculated is basic and it was from this flat plate theory that the following theory was developed.

By assuming purely axial flow the author has developed the theory by a force balance on an elemental volume next to

the heated surface. This theory includes the definitions for various hydrodynamic and thermal boundary layer thicknesses, included is the enthalpy thickness which is the thermal equivalent to kinetic energy thickness in hydrodynamic boundary layer theory.

The work itself requires temperature and velocity profiles to be taken at various points downstream from the leading edge of the flat plate. The other boundary layer thicknesses are found by ratios and graphical integration. This yields parameters which can be substituted into the equation for the heat transfer coefficient or the Stanton number.

The plate used was the bottom of a rectangular duct and roughened by a powder metallurgical process which left a pebbled but porous surface which had to be sealed against air flow from below. The temperature and velocity profiles were not taken simultaneously, with the velocity profiles being taken when no heat was being applied to the surface. The temperature profiles were taken by a probe consisting of one calibrated thermocouple.

In the development of the theory the author obtained equations for both the local and the mean overall heat transfer coefficient. For some reason the local values were not calculated, which was unfortunate and could easily have been reported since all the parameters had been calculated.

Instead, growth of the boundary layers is shown by the change in the mean or overall heat transfer coefficient as the points at which the profiles were taken increased from the leading edge.

3.1 THE RELATION BETWEEN THE TOTAL APPLIED ENERGY AND THE BOUNDARY LAYER

A cylindrical isothermal surface of temperature t_w around which was flowing a perfect gas was considered. It was assumed in the temperature range considered, that the specific heats were constant. Also, it was assumed that there was no swirl and that static pressure did not vary normally to the surface.

In the diagrams AB and CD are finite lengths equal to the hydrodynamic boundary layer thickness at point A and C respectively. These points are separated in the axial direction by a unit length dx. The control volume (dV) was formed by the two sides A, B, C, D, and A', B', C', D'.

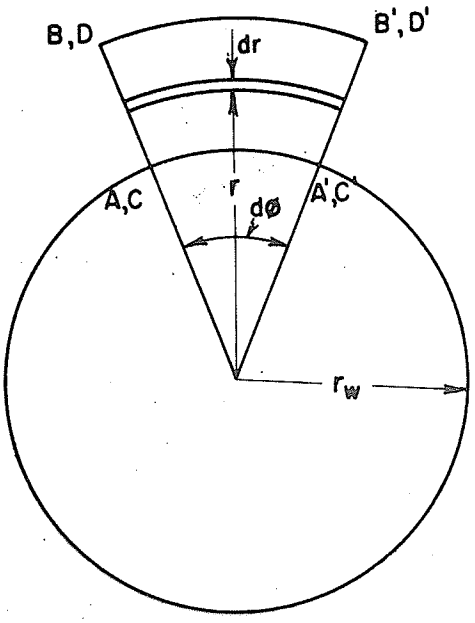

The mean height of the hydrodynamic boundary layer along the length dx was considered equal to Δ and u_Δ the gas velocity at this height.

Under non-steady state conditions the variation (dE) of the total energy (E), which is the sum of the internal and kinetic energy of dV at time θ, was equal to the change

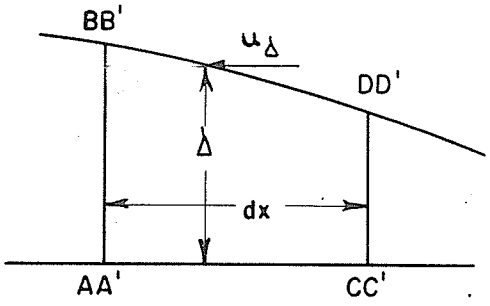

of work dW and heat dQ in the control volume in a unit time dθ.

The change in total energy with respect to time was written:

$$\frac{dE}{d\theta} = dW + dQ$$

The energy transported by the fluid in the boundary layer, which in a unit time, crossed the surface normal to the flow at a distance r from the centre and having dimensions equal to the dimensions of elementary height dr was

$$\left(\frac{u^2}{2} + Cvt\right) \rho urdrd\varphi \qquad \ldots\ldots\ldots\ldots\ldots\ldots \quad 3.1$$

Taking into account the energy which enters the volume dV by the surfaces AB and BD, and leaves the surface CD in a unit time:

$$dE = dx \left[\frac{d}{dx} \int_{r_w}^{r_w+\Delta} \left[\left(\frac{u^2}{2} + Cvt\right)\rho urd\varphi\right] dr \right.$$

$$\left. - \left(\frac{u\Delta^2}{2} + Cvt\Delta\right) \frac{d}{dx} \int_{r_w}^{r_w+\Delta} \rho urdrd\varphi\right] \qquad \ldots\ldots\ldots\ldots \quad 3.2$$

The integral limits can be changed from r_w and $r_w + \Delta$ to 0 and Δ since the integral approaches zero as the limit

approaches r_w. The upper limit is left at $\acute{\Delta}$ since the thermal boundary layer thickness was less than or, at most, equal to the hydrodynamic thickness since heating did not start at the leading edge and the Prandtl number was nearly equal to 1.

There was no relative displacement of the fluid in contact with the surface so that there was no work done by the forces of friction applied on the surface AC. Similarly, the velocity gradient was very small on the surface BD, and so there was no work done by friction forces on this surface. Finally, the only applied forces which are doing any work are the pressure forces on the surfaces AB, CD, and BD. If "p" was the pressure at a point a distance '$r-r_w$' from the surface and $p_{\acute{\Delta}}$ the pressure at distance $\acute{\Delta}$, the sum of the work done by the applied forces on the volume in a unit time was written.

$$dW = dx \left[\frac{p\acute{\Delta}}{\rho\acute{\Delta}} \frac{d}{dx} \int_o^{\acute{\Delta}} \rho u r dr d\varphi - \frac{d}{dx} \int_o^{\acute{\Delta}} \rho u r dr d\varphi\right] \quad \ldots\ldots\ldots\ldots\ldots \quad 3.3$$

The only quantity of heat dQ which entered the volume dV was that which crossed the bottom through surface element AC. If Φ designates the flux density at the surface:

$$dQ = dx \; r_w d\varphi \; \Phi_p$$

Since a perfect gas was assumed.

$$C_v t + \frac{p}{\rho} = C_p t$$

Taking an energy balance of the initial relations and using the expansion of a differential product the following was obtained:

$$\Phi_w = \frac{1}{r_w} \left[\frac{d}{dx} \int_0^{\Delta} \left(\frac{u^2}{2} + C_p t \right) \rho u r dr \right.$$

$$- \frac{d}{dx} \left(u_{\Delta}^2 + C p t_{\Delta} \right) \int_0^{\Delta} \rho u r dr$$

$$\left. + \left(u_{\Delta} \frac{du_{\Delta}}{dx} + C_p \frac{dt_{\Delta}}{dx} \right) \int_0^{\Delta} \rho u r dr \right] \qquad \ldots\ldots\ldots\ldots 3.4$$

The equation for the conservation of energy was written for the flow at the upper limit of the boundary layer.

$$\frac{u_{\Delta}^2}{2} + C p t_{\Delta} = \text{CONST.}$$

$$u_{\Delta} \frac{du_{\Delta}}{dx} + Cp \frac{dt_{\Delta}}{dx} = 0 \qquad \ldots\ldots\ldots\ldots\ldots\ldots\ldots 3.5$$

From the above equation the last term of equation 3-4 equals zero.

For annular flow the upper limit of the integration was left as Δ but equation 3-4 was further simplified to give

$$\Phi_w = \frac{1}{r_w}\left[C_p \frac{d}{dx}\int_0^{\Delta}(t-t_{\Delta})\rho u r dr - \frac{d}{dx}\int_0^{\Delta}\frac{(u_{\Delta}^2-u^2)}{2}\rho u r dr\right] \quad \ldots\ldots\ldots\ldots 3.6$$

$$\text{Let } \Delta_3 = \int_0^{\Delta}\frac{u}{u_{\Delta}}\left(1-\frac{u^2}{u_{\Delta}^2}\right)\left(\frac{r}{r_w}\right)\left(\frac{\rho}{\rho_{\Delta}}\right) dr \quad \ldots\ldots\ldots\ldots\ldots 3.7$$

This was considered the kinetic energy thickness for an annulus.

$$\text{Let } \Delta_{t_2} = \int_0^{\Delta}\frac{u}{u_{\Delta}}\left(\frac{t-t_{\Delta}}{t_w-t_{\Delta}}\right)\left(\frac{r}{r_w}\right)\left(\frac{\rho}{\rho_{\Delta}}\right) dr \quad \ldots\ldots\ldots\ldots 3.8$$

This was considered the enthalpy thickness for an annulus.

Equation 3.6 could then be rewritten

$$\Phi_w = \left[C_p \frac{d}{dx}(t_w-t_{\Delta})p_{\Delta}u_{\Delta}\Delta t_2 - \frac{1}{2}\frac{d}{dx}(\rho_{\Delta}u^3\Delta_3)\right] \ldots\ldots 3.9$$

Finally, in the case of the annular area for t_{Δ} and ρ_{Δ} equal to a constant.

$$\Phi_w = C_p\rho_{\Delta}\left[(t_w-t_{\Delta})\frac{d}{dx}(u_{\Delta}\Delta_{t_2}) - \frac{1}{2C_p}\frac{d}{dx}(u_{\Delta}^3\Delta_3)\right] \quad \ldots\ldots\ldots\ldots\ldots 3.10$$

3.2 CALCULATION OF THE CONVECTIVE HEAT TRANSFER COEFFICIENTS

When a body is immersed in a flowing fluid, the fluid is heated due to the dissipation of energy in the boundary layer and assumes a temperature t_f greater than the free stream temperature t_o. However, in this case the temperature of the body was relatively high and the velocities relatively low so that this friction heating was neglected.

The convective heat transfer coefficient can be described as

$$h = \frac{\Phi_p}{t_w - t_\delta} \quad \text{..... 3.11}$$

Then by equating 3.10 and 3.11 the following was obtained.

$$h = C_p \rho_\delta \left[\frac{t_w - t_\delta}{t_w - t_\delta} \frac{d}{dx} (u_\delta \Delta t_2) - \frac{1}{2C_p(t_w - t_\delta)} \frac{d}{dx} (u_\delta^3 \delta_3) \right] \quad \text{..... 3.12}$$

or

$$h = C_p \rho_\delta \left[\frac{d}{dx} (u_\delta \Delta t_2) - \frac{1}{2C_p(t_w - t_\delta)} \frac{d}{dx} (u_\delta^3 \delta_3) \right] \quad \text{.... 3.13}$$

Giving the results in terms of the Stanton Number:

$$NST = \frac{h}{C_p \rho \delta' u_\delta'} = \frac{1}{u_\delta'} \left[\frac{d}{dx} \left(u_\delta' \delta_{t_2}' \right) - \frac{1}{2C_p (t_w - t_\delta)} \frac{d}{dx} \left(u_\delta^3 \delta_3' \right) \right] \quad \ldots\ldots\ldots\ldots \quad 3.14$$

Then $\frac{d}{dx} (u_\delta' \delta_{t_2}')$ and $\frac{d}{dx} (u_\delta^3 \delta_3')$ were evaluated by determining δ_{t_2}' and δ_3' from the temperature and velocity profiles taken at points along the length of the test section and determining their slope from a graph.

A uniform temperature distribution along the test section of the pipe from L_1 to L_2 was assumed.

$$Q = \int_{L_1}^{L_2} \Phi_w dx = C_p \rho \delta' u_\delta' \left[(t_w - t_\delta) \delta_{t_2}' - \frac{u_\delta^2}{2C_p} \delta_3' \right]_{L_1}^{L_2} \quad \ldots\ldots\ldots\ldots \quad 3.15$$

The mean flux density along the length $L_2 - L_1$ was obtained as shown:

$$\Phi_{wm} = \frac{Q}{L_2 - L_1} = C_p \rho \delta' u_\delta' \left[(t_w - t_\delta) \frac{(\delta_{t_2} L_2 - \delta_{t_2} L_1)}{L_2 - L_1} - \frac{u_\delta^2}{2C_p} \frac{\delta_3 L_2 - \delta_3 L_1}{L_2 - L_1} \right] \quad \ldots\ldots\ldots\ldots \quad 3.16$$

Here Q = heat transfer per unit width.

The mean convective heat transfer coefficient was defined as:

$$h_m = \frac{\Phi_{wm}}{t_w - t_{\Delta}'}$$

and the mean Stanton number by:

$$NST_m = \frac{h_m}{C_p \rho_{\Delta}' u_{\Delta}'}$$

Hence:

$$h_m = C_p \rho_{\Delta}' u_{\Delta}' \left[\frac{\Delta_{t_2} L_2 - \Delta_{t_2} L_1}{L_2 - L_1} - \frac{u_{\Delta}^2}{2C_p (t_w - t_{\Delta}')} \frac{\Delta_{3} L_2 - \Delta_{3} L_1}{L_2 - L_1} \right] \quad \ldots\ldots\ldots \quad 3.17$$

$$NST_m = \frac{\Delta_{t_2} L_2 - \Delta_{t_1} L_1}{L_2 - L_1} - \frac{u_{\Delta}^2}{2C_p (t_w - t_{\Delta}')} \frac{\Delta_{3} L_2 - \Delta_{3} L_1}{L_2 - L_1} \quad \ldots\ldots\ldots \quad 3.18$$

Equations 3.17 and 3.18 are methods to obtain the average heat transfer coefficient from thermal and hydrodynamic boundary layer profiles while equation 3.13 gives the local heat transfer coefficient at any desired point. Graphical integration rather than numerical integration was used to evaluate the kinetic energy and enthalpy thickness.

CHAPTER 4

DESCRIPTION OF APPARATUS

In the previous chapter equations were developed so that the heat transfer coefficients could be obtained from profiles of the thermal and hydrodynamic boundary layers. This chapter is devoted to the description of the apparatus used to obtain experimental results.

4.1 THE AIR SUPPLY

The air supply was a two stage radial vane compressor connected through a fluid coupling to a six cylinder Perkins diesel engine. The diesel ran at a constant speed of 1100 rpm with the compressor speed up to 10,000 rpm. The speed of the compressor was controlled by adjusting the oil level in the fluid coupling.

Air flow was out of the compressor, through a water cooled radiator and into the surge tank shown in figure 3.

4.2 THE OUTSIDE SECTION

The outside of the annular section was a six and one half foot length of six inch nominal diameter pipe as shown in figure 3. On a horizontal plane through the central axis the static pressure taps were located. These taps were located directly opposite one another starting eight inches from the

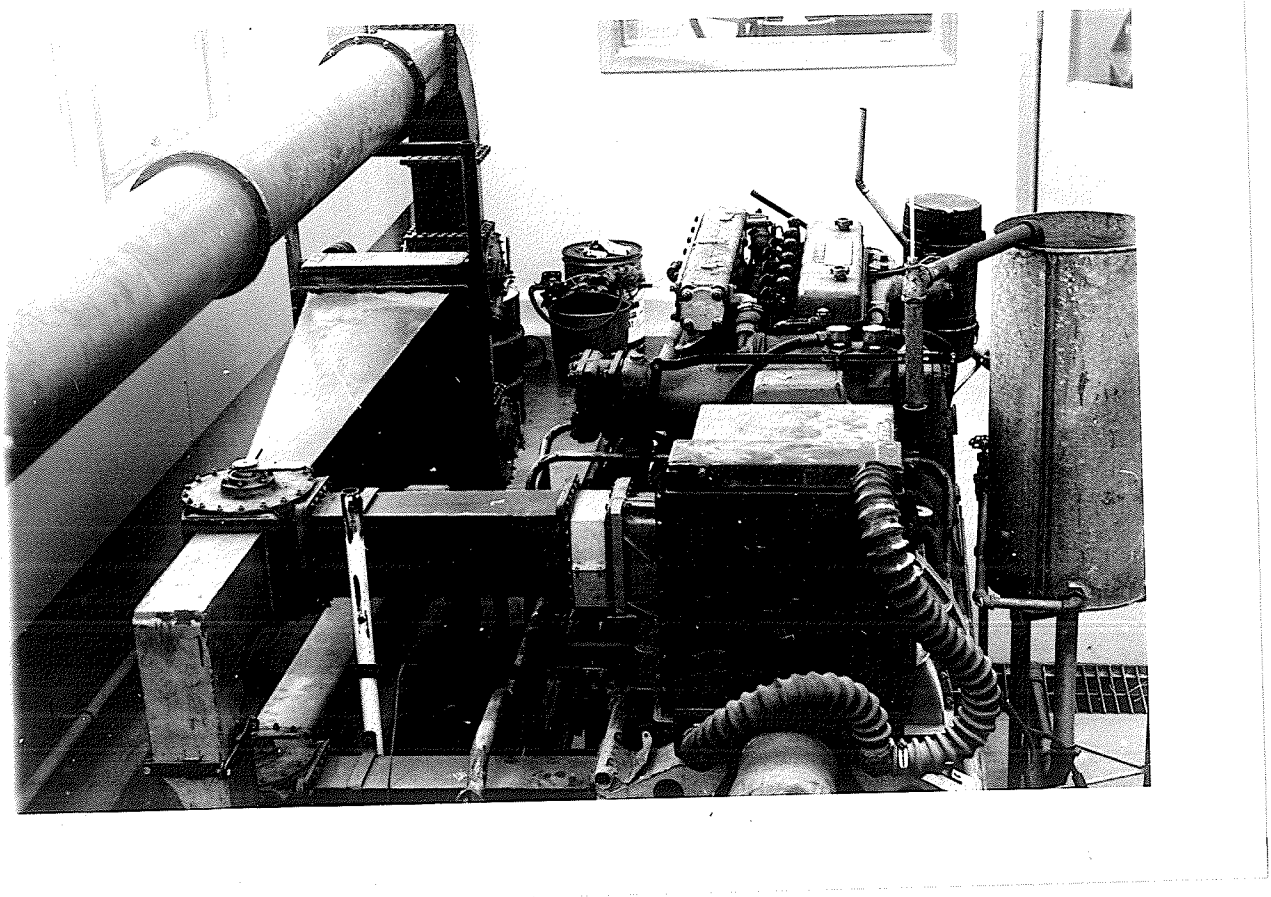

FIGURE 1. AIR SUPPLY CENTRIFUGAL FAN AND DIESEL ENGINE

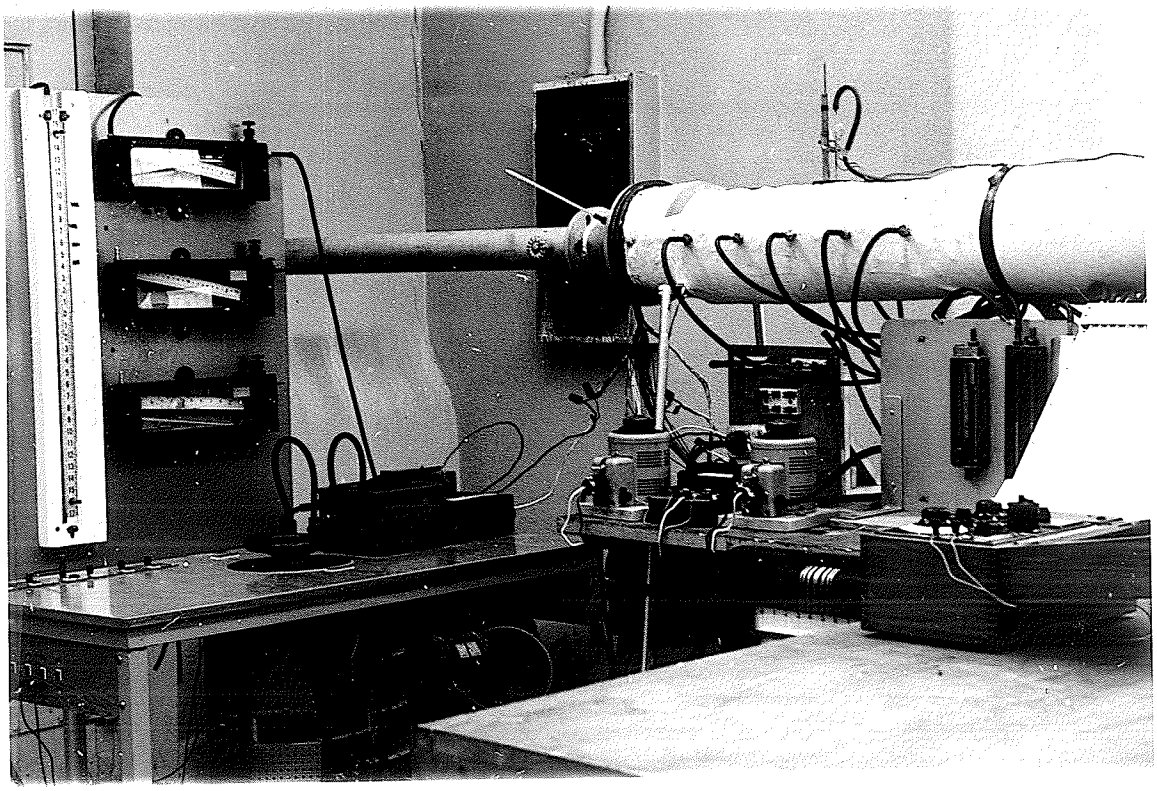

FIGURE 2. TEST SECTION. DOWNSTREAM END OF ANNULUS AND MEASURING INSTRUMENTS

downstream end and in five inch increments for twenty inches. This made ten pressure taps which were connected by rubber tubing to a multibank inclined manometer. The manometer was filled with silicone (S.G.=1) fluid and inclined at an angle of approximately 45° so that one inch on the manometer equalled 0.725 inches of water. To ensure that there was no roughness on the inside of the pressure taps the inside of the holes were ground slightly with a small electric drill using dentists bits.

In order to allow the entrance of the pressure-temperature probe into the annulus a 3/16 x 22 inch slit was cut in the top of the outside section starting seven inches from the downstream end. Before this slit was cut the two angle irons shown in section B.B. of figure 3 were welded in place, the entire six foot six inch section was then clamped in position on the bed of a milling machine and the slit milled. After the slit had been cut the sides and top of the angle irons were milled to give an accurate base for the pressure-temperature probe assembly. The inside of the slit was then finished with the small electric drill mentioned previously.

The air seal around the slit was obtained by inserting two 5/8 inch foam rubber tubes between the pipe and the angle irons. A tight fit between these foam rubber tubes was ensured by inserting a piece of 3/16 x 1/2 x 22 inch metal strapping along the vertical leg of each angle iron.

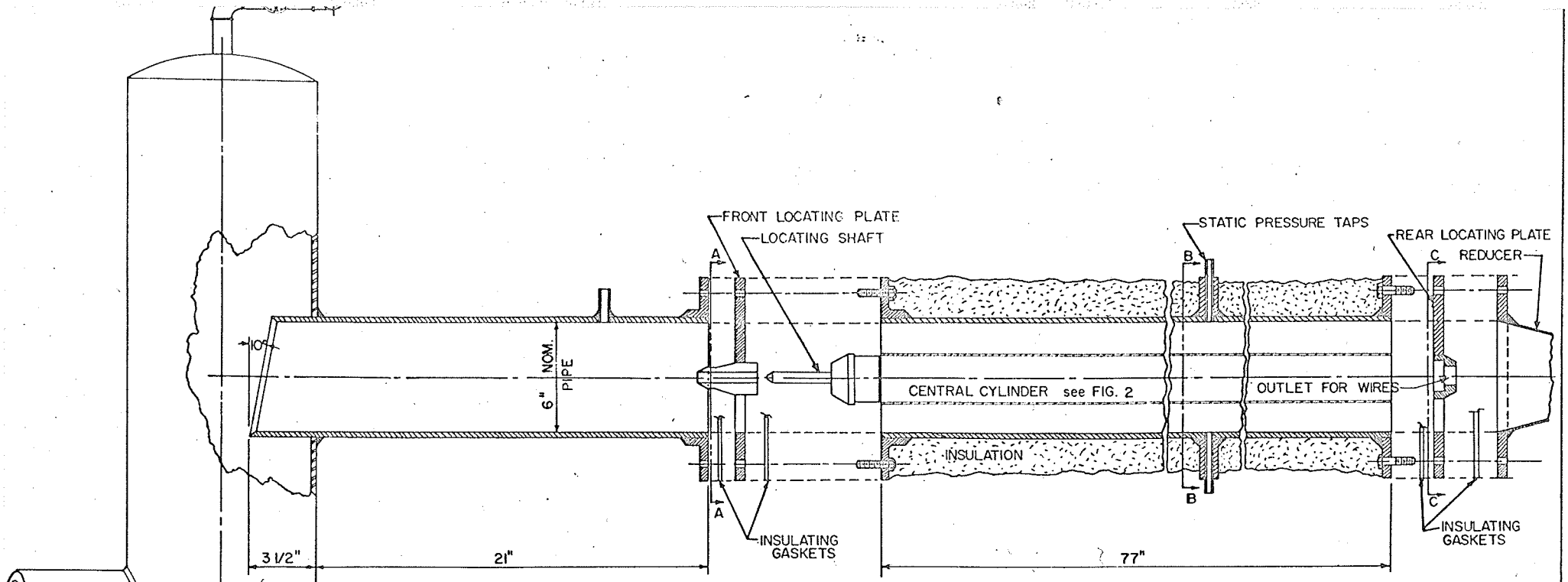

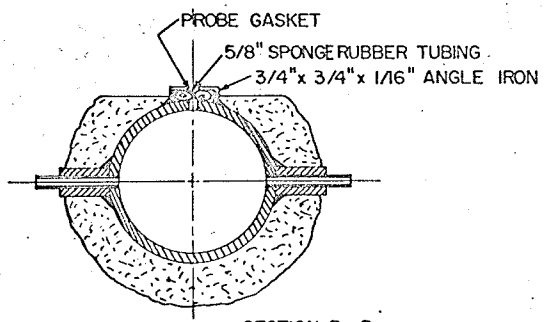

SECTION B–B

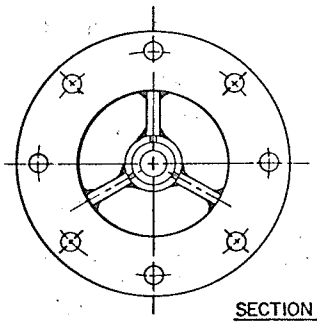

SECTION C–C

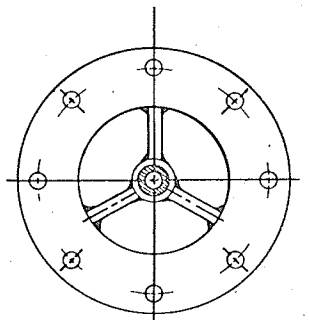

SECTION A–A

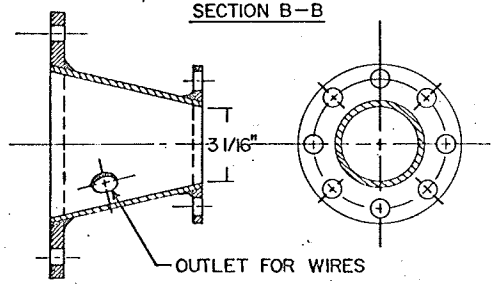

DETAIL OF REDUCER

UNIVERSITY OF MANITOBA DEPT. OF MECHANICAL ENGINEERING			
DRAWN		SCALE:	
DATE	JULY 20.1963	1/4" = 1"	
APPROVED			
SURFACE ROUGHNESS TEST RIG		FIG. NO. 3	

With the exception of the angle iron, the entire outside of the pipe was then covered with two inches of fiberglass insulation. In order to make an air seal at the ends of the slit, putty was packed against the angle irons and built up to meet the insulation. The putty was held in position by an adhesive tape which is commercially used as an air seal.

The two flanges were welded on either end of the test section to complete the fabrication of the outer section.

4.3 THE TEMPERATURE-PRESSURE PROBE

The temperature-pressure probe was as shown in Figure 4. The base of the probe was fabricated of mild steel with the inside faces being machined and polished. Attached to this base was a modified set of calipers. The fixed jaw of these calipers was removed, drilled and tapped and used as a clamp on the moving jaw. The exposed end of the calipers was then brazed to the middle of the base.

The pressure section of the probe was made from number eighteen gauge stainless steel hypodermic needle tubing. A hole 0.030 inches in diameter was drilled approximately 1/4 inch from the end of the tubing and normal to the central axis. To block the end of the tubing closest to the hole a cleaning rod was inserted in the tubing to a point just past the hole and the remaining length filled with silver solder.

DETAIL OF PRESSURE- TEMPERATURE PROBE.

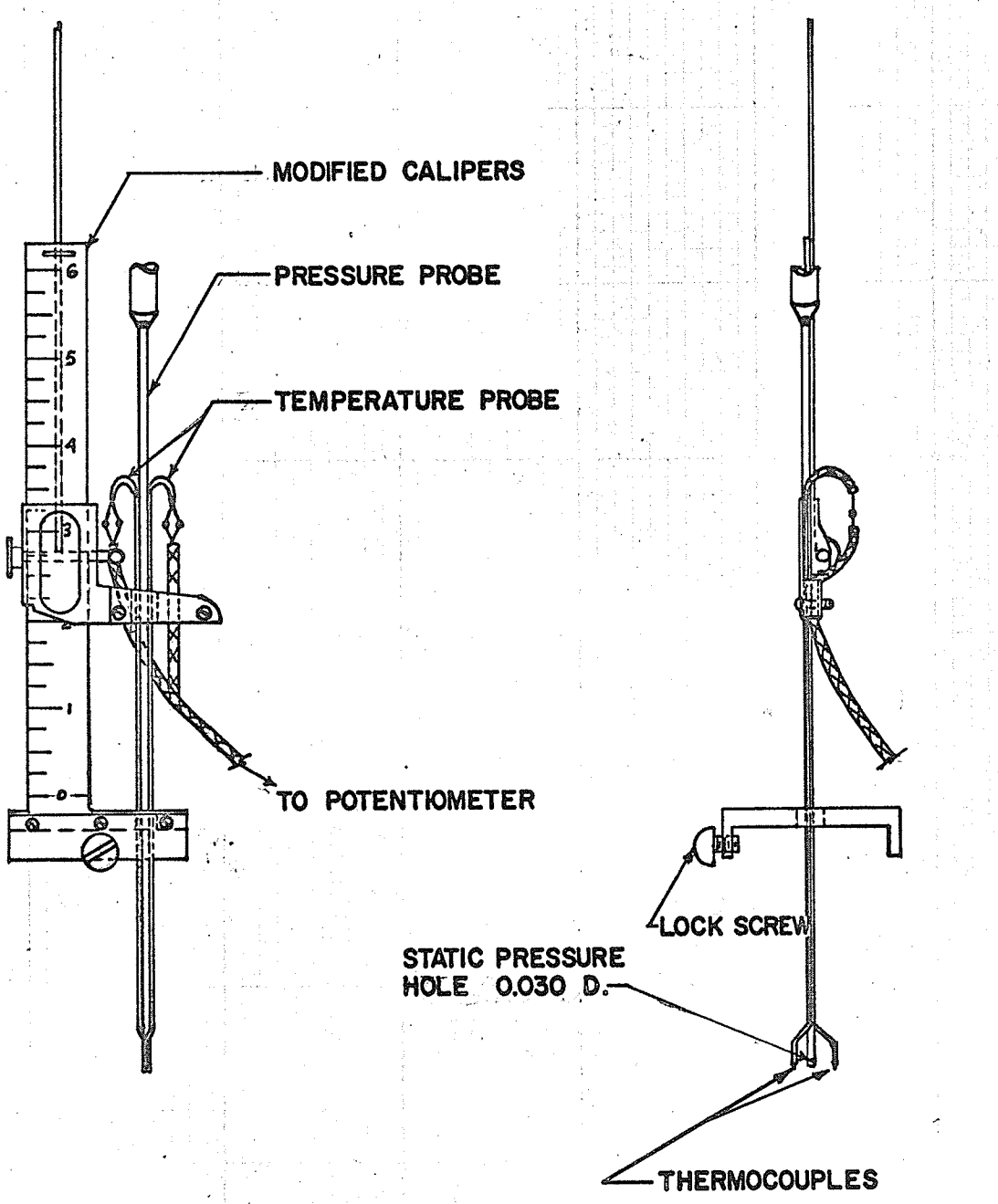

FIG.NO. 4.

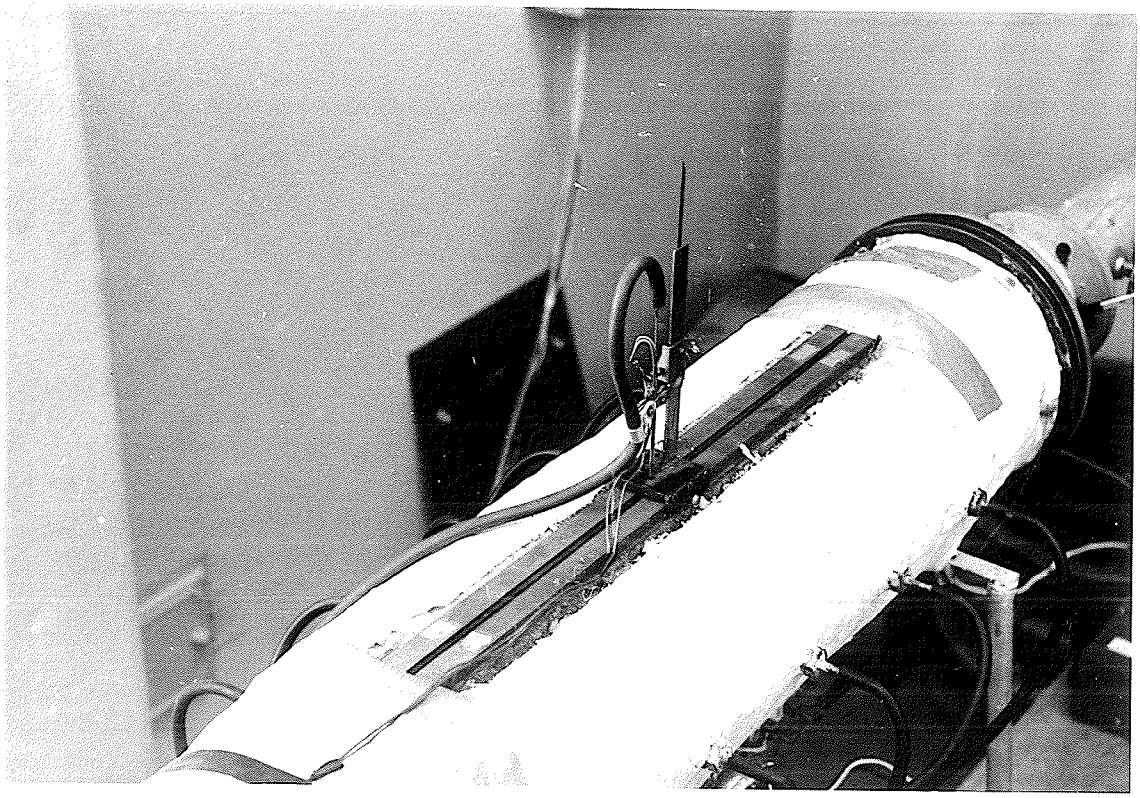

FIGURE 5. PROBE IN POSITION OVER TEST SECTION.

The filled end was then ground down as much as possible, which left the centre of the hole 0.029 inches from the bottom of the probe, this distance being measured on a microscope with a vernier lense.

Since the readings were desired directly in velocity pressure a static pressure tube was led from the outside section closest to where the profile was being taken. The leads from the total and static pressure were connected to an inclined manometer filled with red meriam and reading to the nearest .01 inches of water.

The temperature section was made from .040 inch stainless steel guarded iron constantan wire which was used since it would retain its shape after being bent. The thermocouple beads were arc welded in an oxygen free atmosphere to ensure a high quality.

The guarded thermocouple wire was then soldered to the pressure section and bent into the shape shown in figure 4. The beads were kept far enough away from the pressure section so that they would not effect the air flow around it. The two thermocouples were then connected in parallel on the assumption that the average temperature at these two points would equal the temperature at the pressure probe. The emf readings for these thermocouples were taken on a portable Cambridge potentiometer which read to the nearest .001 millivolts.

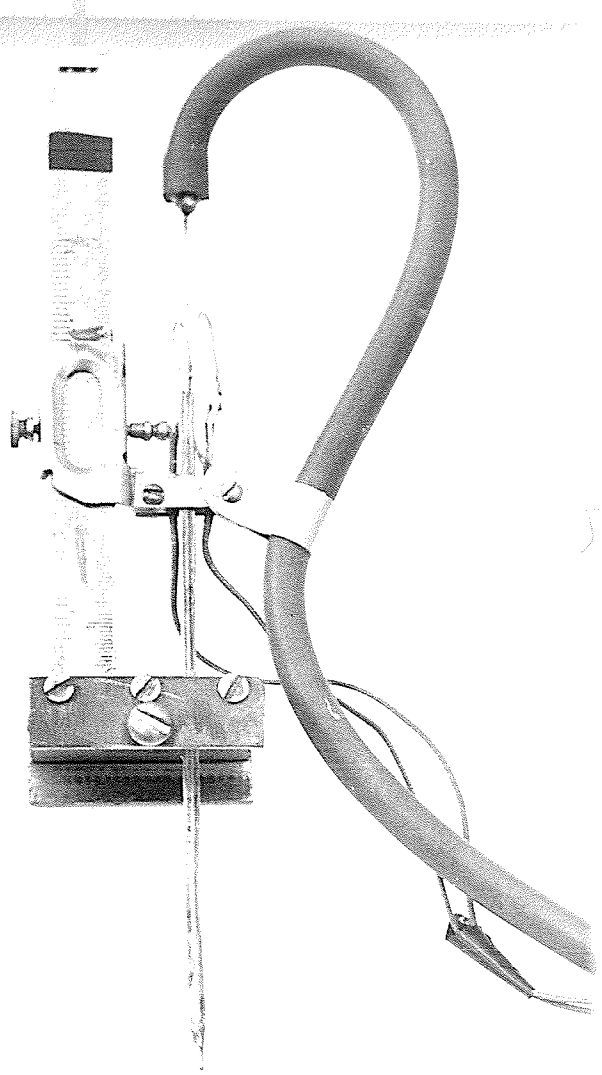

FIGURE 6. PRESSURE-TEMPERATURE PROBE

4.4 THE CENTRAL SECTION

The central section of the annular area was made up of two separate parts, the entrance length and the test section. The entrance length was common to all the test sections and was 40½ inches long. This section was made of two inch nominal diameter pipe cut to 2.30 inches O.D. The front of the entrance length was centred by the support flange shown in figure 3. The test sections were connected by the pin as shown in figure 3 as well as spot welding for extra rigidity. Any irregularities in the connection between these two sections was removed by profiling the joint with a thin layer of T-3 thermon cement.

Inside the test section three heaters were located. These consisted of two eight inch 1.5 KW heaters located at either end and one 4 KW heater located in the middle of the test section. These heaters were shaped as shown in figure 7, and forced against the walls by a central support cylinder, which was merely a piece of pipe cut to fit snugly inside the heaters. Power was supplied to the heaters through wattmeters as shown in figure 8, which metered the power to the guard heaters as well as the central test section, the current being regulated by the three variacs.

DETAIL OF HEATERS

SECTIONS AND ENTRANCE LENGTH.

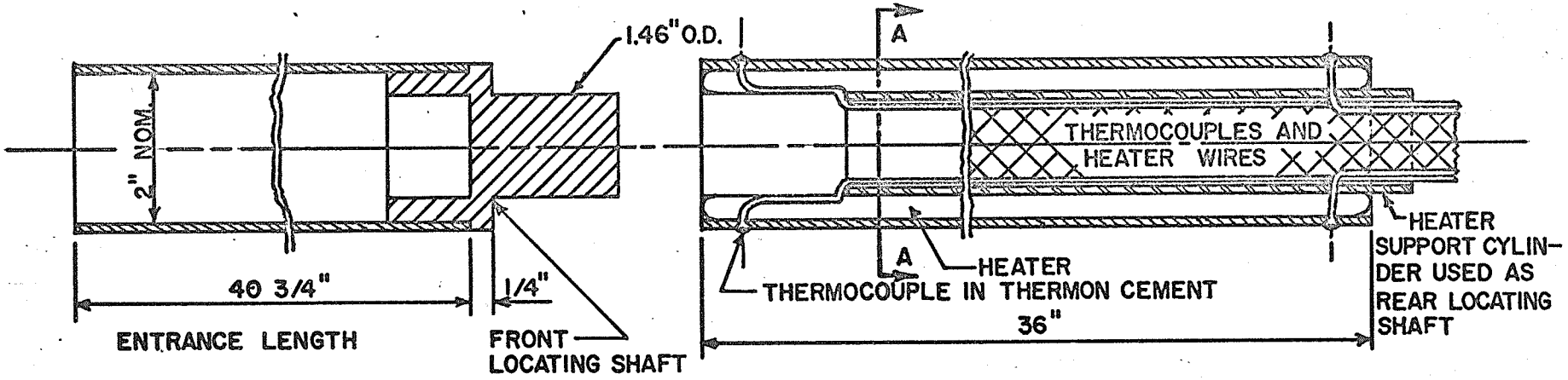

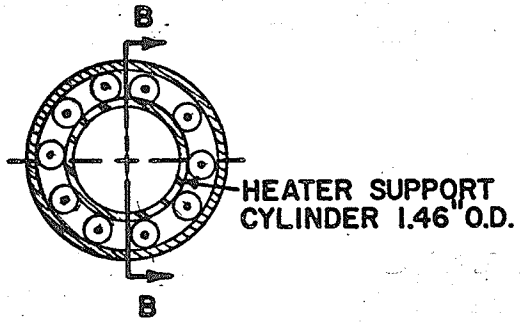

SECTION A-A

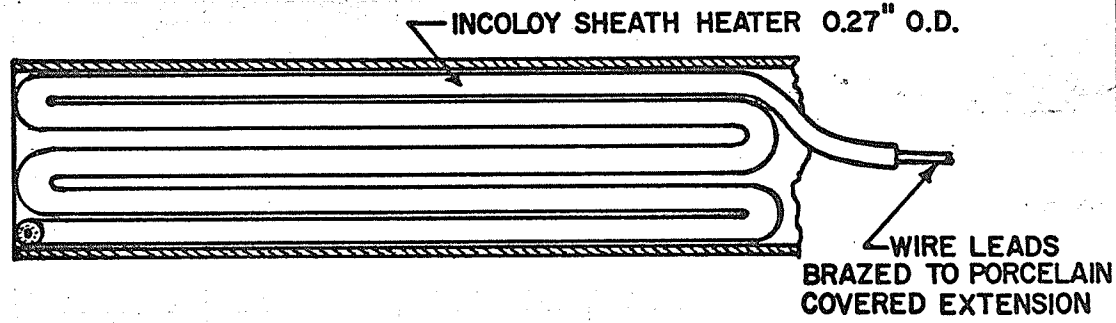

SECTION B-B

(HEATER SUPPORT CYLINDER NOT SHOWN)

HEATERS 2 OFF 1.5 KW INCOLOY SHEATH 115 V. 8" LONG
1 OFF 4 KW INCOLOY SHEATH 208 V. 20" LONG

FIG. NO. 7.

SCALE: 1/2" = 1"

SCHEMATIC DIAGRAM OF HEATER CIRCUITS

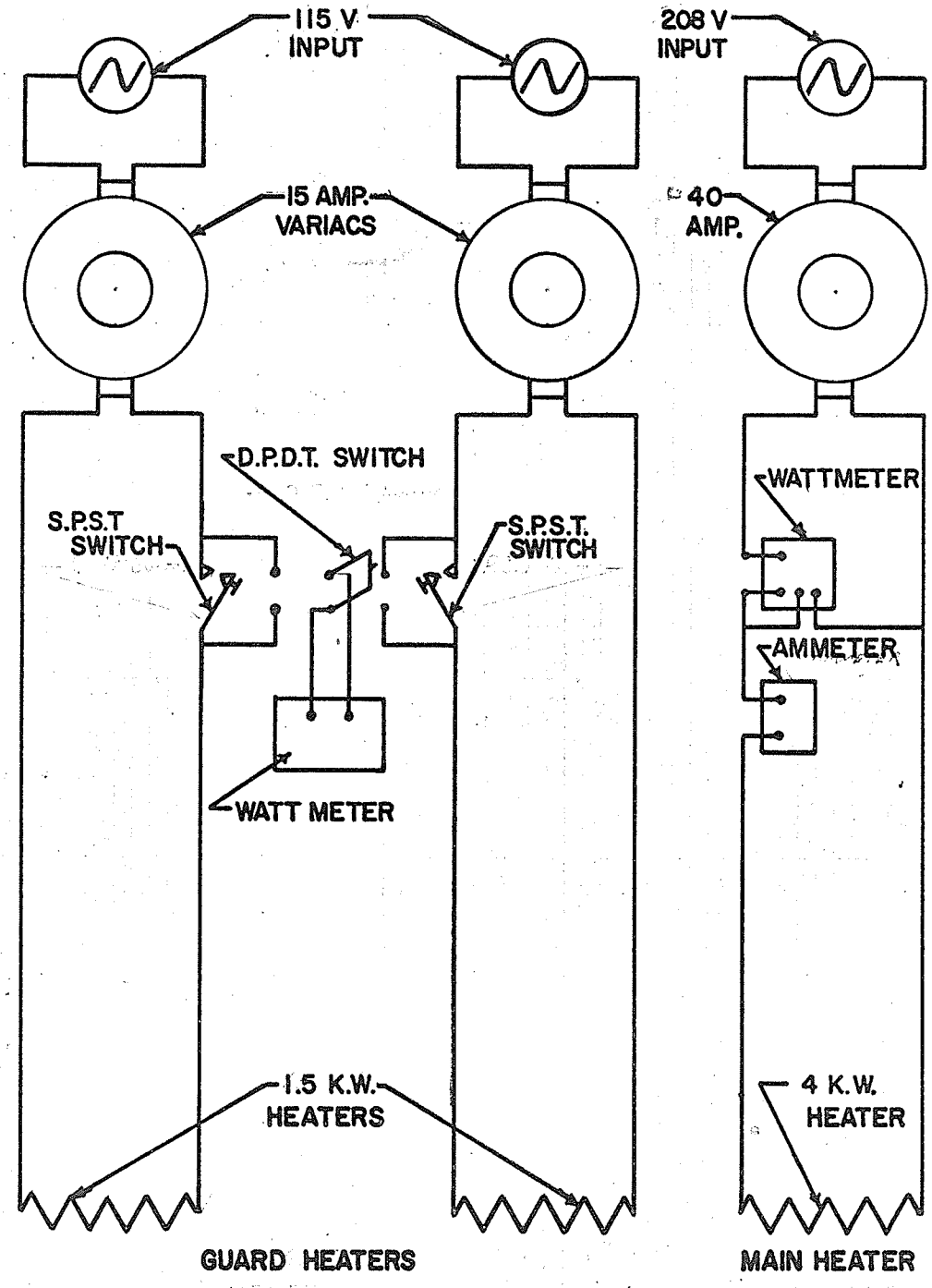

N.T.S.

FIG. NO. 8 .

4.5 THE TEST SECTIONS

In attempting to obtain a random roughness for the test sections several methods were considered. One of these was to cause grain growth and carbon precipitation on the cylinder and dispose of the inter-grain material by etching. In order to find the approximate order of grain size that could be obtained samples of stainless steel were prepared and heat treated.

Six samples were cut from available 304 stainless steel stock and lettered A to F. All the samples were polished before heat treatment, and then given a light polish after. Samples A and B were heated in the furnace at 1300°F for a period of fifty minutes. The samples were then etched by sulphuric acid and observed under the microscope. There was very little or no grain growth in these two samples with some of the carbide precipitating, and the rest remaining in the grains as nodules.

Sample C was heated in the furnace at a temperature of 1600°F for one hour, then etched as before and observed under the microscope. A very definite increase in grain size was noted, this being from a value of less than 0.001 inches to around 0.002 inches. Most of the carbon had precipitated but some carbon nodules remained in the grain.

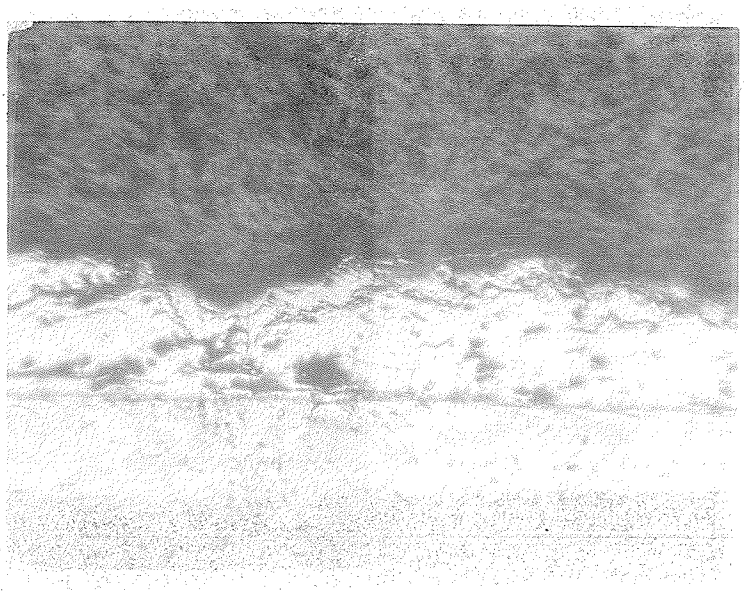

FIGURE 9. BOND BETWEEN PIPE AND STAINLESS STEEL (X 66)

Samples D and E were both heat treated at a temperature of 1600°F, sample D was in the furnace for a period of 3 hours, and sample C for four. Another definite increase was noted in the grain size with sample D having a grain size of 0.003 inches and sample E a grain size of 0.004 inches. In these two samples most of the carbon had precipitated to the grain boundaries and it did not appear that grain sizes of the desired magnitude could be obtained without considerable difficulty and expense.

For these reasons any attempts to obtain a surface roughness by grain growth were abandoned in favour of metallizing the surface with stainless steel and machine roughening.

Figure 9 shows a photograph of the bond between the parent metal and the stainless steel. There are some inclusions between the parent metal and the stainless steel which are probably due to the bonding material which was sprayed on the pipe prior to metallizing it with the stainless steel. The inclusions or air pockets through the stainless steel probably come from the method of application.

The surface obtained was the roughest possible by this method as any faster rate of feed into the metallizing gun caused the metal to deposit itself in large pieces on the surface. These pieces made it impossible to deposit a uniform thickness on all parts of the pipe and had a very poor bond

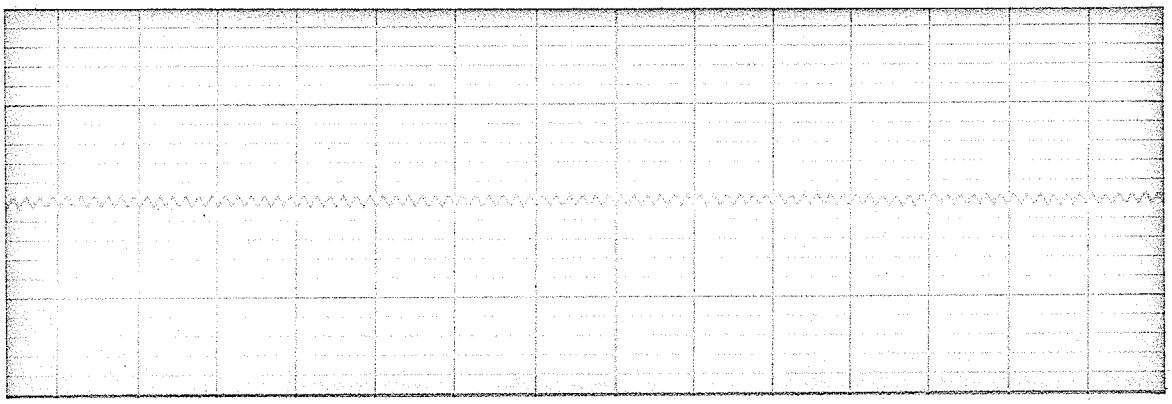

EXTRANEOUS 60 CYCLE PICKUP

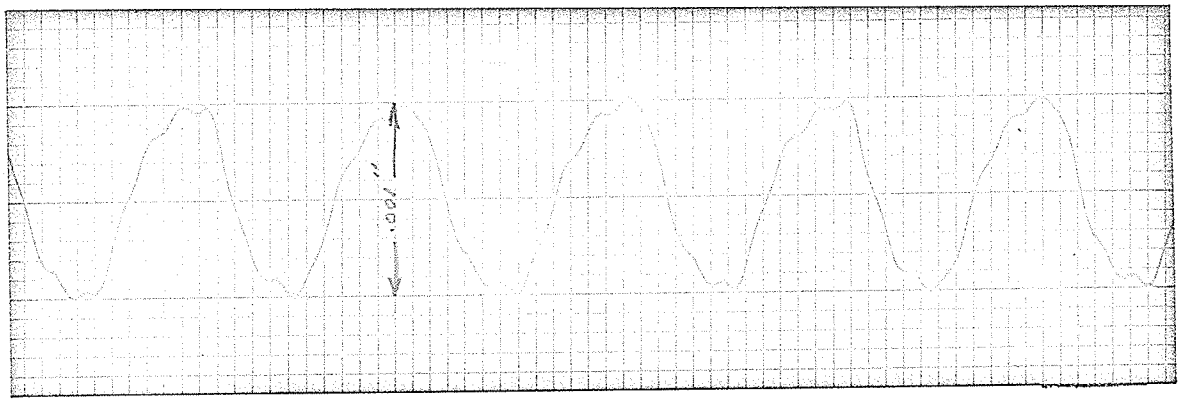

STANDARD SAMPLE CALIBRATION

FIGURE 10

VISICORDER TRACES OF TEST SECTIONS

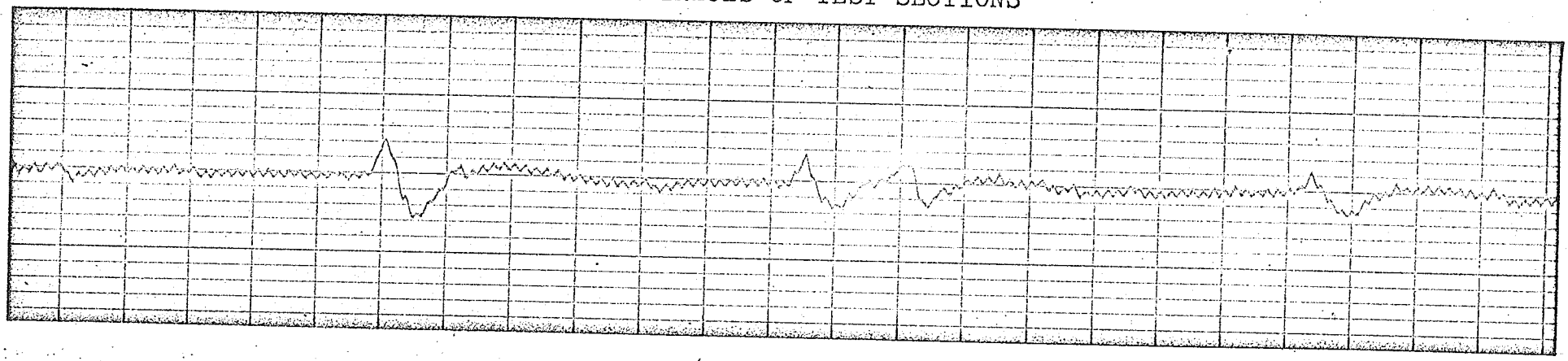

FIGURE 11

MACHINED SMOOTH TUBE

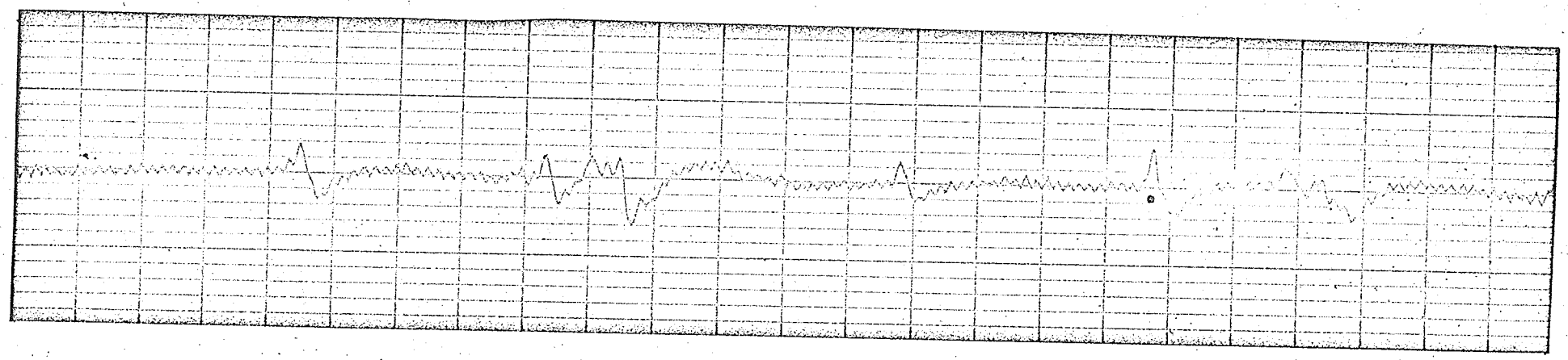

FIGURE 12

STAINLESS STEEL COATED SMOOTH TUBE

VISICORDER TRACES OF TEST SECTIONS

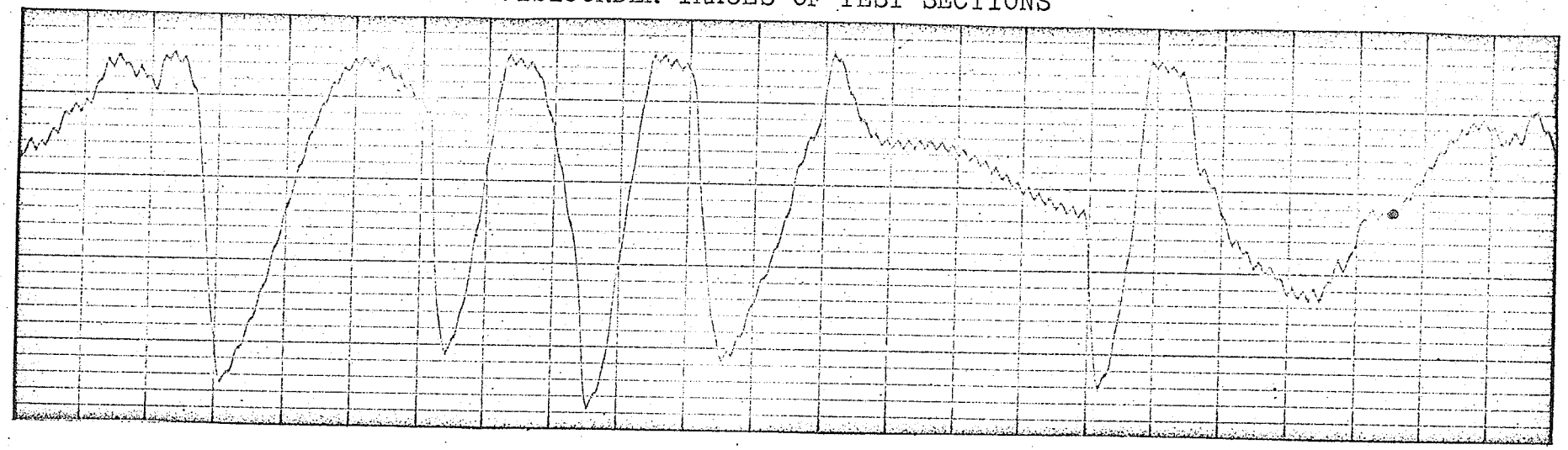

FIGURE 13

KNURLED AND THREADED TUBE

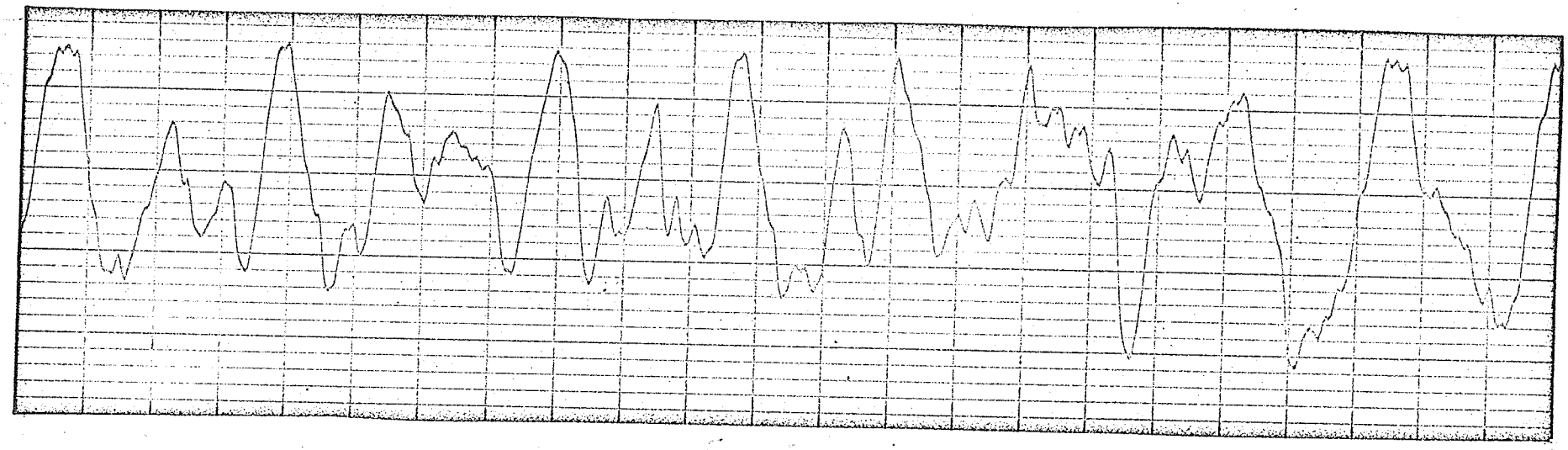

FIGURE 14

STAINLESS STEEL COATED ROUGH TUBE

which would fail under the slightest mechanical loading.

Four test sections were prepared, two by the metallizing method and, two by machine roughening. Of the two stainless steel coated tubes one was left in the rough state and the other was smooth and polished. There were also one smooth and one roughened tube not coated with stainless steel, the rough tube was threaded with threads 0.020 inches deep at a pitch of 18 to the inch. The diameter of all the tubes was taken as 2.30 inches, this being the diameter of the smooth tubes and considered the mean diameter of the rough ones.

The surface roughness of all the tubes was measured by Brüel and Kjoer surface roughness equipment using a diamond stylus which had a 500 microinch radius, the stylus being calibrated against a standard roughness supplied with the equipment. The height of this standard sample roughness was 0.001 inches, peak to base. This distance was set equal to one inch of travel on the Honeywell visicorder which was used to record the roughness.

Figures 10,11,12,13 and 14 show the traces obtained for the four tubes as well as a trace of the standard sample and 60 cycle pickup. The trace for the knurled tube is not considered to be representative of the surface roughness since the stylus did not move over the peaks of the knurling but stayed in the grooves picking up the threaded roughness that

had been placed on the surface prior to knurling. These traces were not used in the calculations but are used as a qualitative analysis of the four surfaces tested. The meter on the Brüel and Kjoer equipment reads the arithmetic mean of the roughness and this was used for the roughness parameter 'e'.

All of the test sections had 18 holes drilled in them as shown in figure 15, this was to allow for the positioning of thermocouple beads on the surface. The thermo couples were made of iron and constantan being secured in position in these holes by T-3 thermon cement. This cement was chosen since it had a thermal conductivity of approximately 25 Btu/hr.ft.°F., which approximates the thermal conductivity of the tube. All the thermocouples were led out of the downstream end of the test section after they came through the central support cylinder which had holes drilled in it to match those in the test section.

The thermocouple beads were all arc welded in an oil on mercury bath using a voltage of 40 volts. The beads were then inspected under a three dimensional microscope to check for any flaws or poor connections. The insulation on these wires had a design limit of 900°F but could not be used twice since the insulation became very weak after a series of tests and could not be laid in the next section without

POSITION OF THERMOCOUPLES ON TEST TUBE

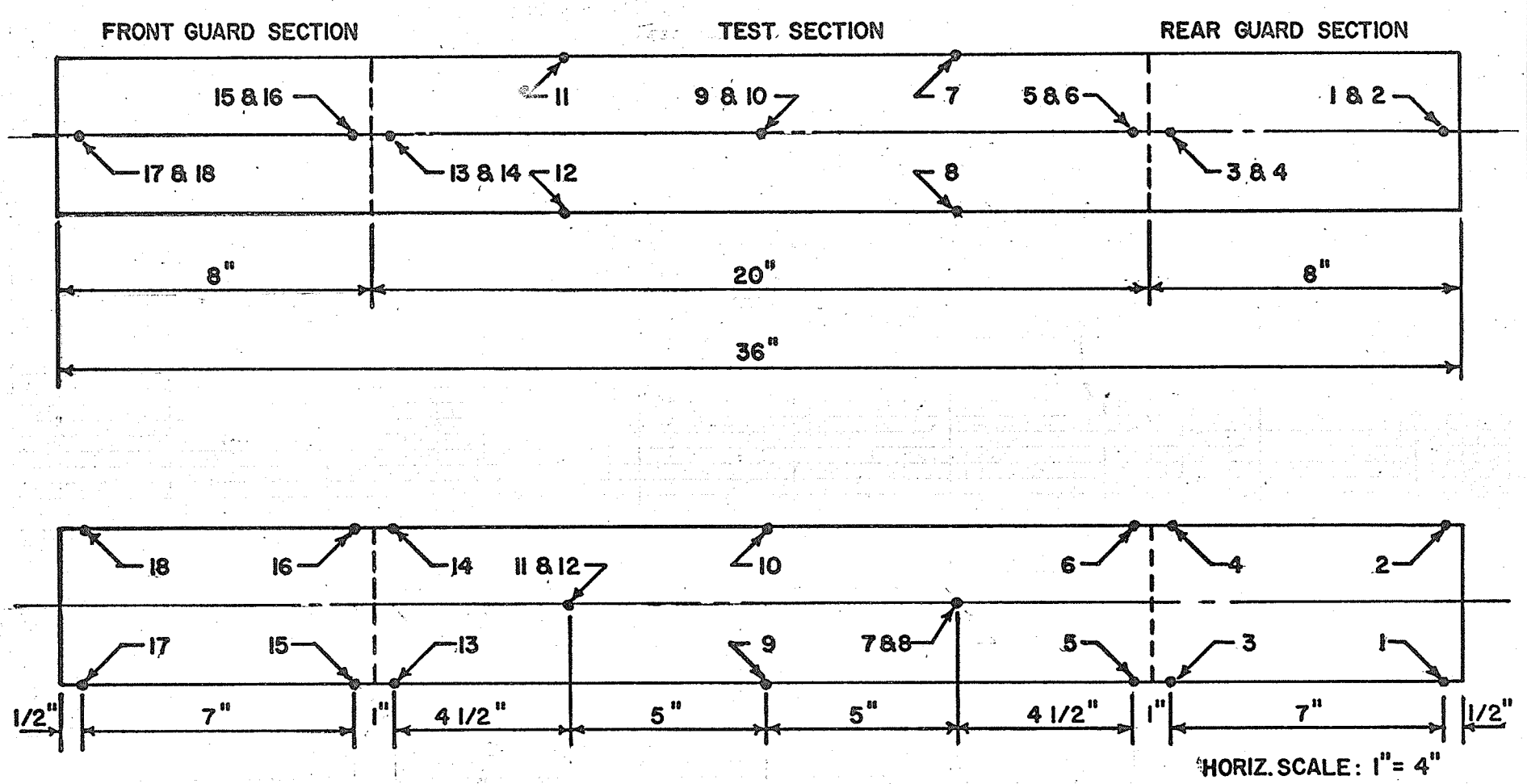

FIG. NO. 15.

being stripped, which meant that new thermocouples had to be made for every test section. The output from these thermocouples was recorded on a Leads and Northrup 16 point recorder, the thermocouples from the guard heaters being paralleled before being connected to the recorder. Referring to figure 15 thermocouples no.1 and 2 were in parallel, similarly 3 and 4, 15 and 16, 17 and 18.

4.6 ASSEMBLY AND TEST PROCEDURE

When the equipment had been assembled as shown in figure 7, initial tests and checks were made on the equipment. The 16 point recorder was calibrated by use of the potentiometer so that offset was reduced to a minimum and oscillation of the self balancing components reduced to approximately one second. The temperature part of the probe was checked against the heat input recorded on the wattmeters as is shown in Appendix 1. The pressure part of the probe was checked against air flow out of the downstream end of the apparatus, where a pitot tube which had been calibrated for previous work was situated.

As a check against any swirl the probe base was raised from the angle irons and the entire probe rotated as much as possible, the pressure section of the probe was then inserted through one of the static pressure holes and rotated, neither of these tests detected any swirl in the system. However, to

reduce chances of swirl occurring, a flow straightener was added to the section in front of the annulus. This straightener was made from one inch nominal diameter furniture tubing and secured in position by a rubber ring.

When a test was to be run the engine was started and brought up to operating temperature with the compressor running at its slowest speed. The air flow was then brought up to a point higher than that desired with final adjustment being made by means of the bleed valve shown in figure 3. The air flow was measured after the reducing section by means of a pitot traverse on the end of the 3 inch nominal diameter pipe.

The temperature of the test sections and both guard heaters were controlled by means of the variacs with the temperature of the guard heaters nearest the test section being adjusted so that it was just equal to or slightly higher than the temperature of the test section as shown in figure 16, which gives a typical profile obtained along the entire length of the test specimen. The power to these heaters was turned on only after the flow had nearly stabilized, complete stabilization of flow and temperature requiring approximately one hour.

The Reynolds number range was kept high so that the effect of the outer wall on the inside hydrodynamic boundary layer would be small. The size of the lowest Reynolds number

to be used was found by running several tests on the smooth stainless steel coated tube until the velocity profile was of a satisfactory shape. The upper value of Reynolds number was dictated only by the capacity of the air supply. This gave a Reynolds number range of from $.8 \times 10^5$ to 1.4×10^5.

Each tube was tested at four Reynolds numbers in the range given above and two temperatures 250° and 350°F. A complete test consisted of taking five temperature and pressure profiles along the test section, reading the wattmeters, the static pressure in the section, the inclined manometer, and a velocity profile at the end of the three inch section. This procedure was completed for each temperature and Reynolds number which made a total of eight tests on each section. The velocity-temperature profiles were taken from as close as possible to the inside tube (0.029 inches) to 30 m.m. from this wall. The profiles were initially taken in millimeters since the inch scale did not have a vernier. The barometric pressure was not taken for each test but periodically during the time a series of tests were being run.

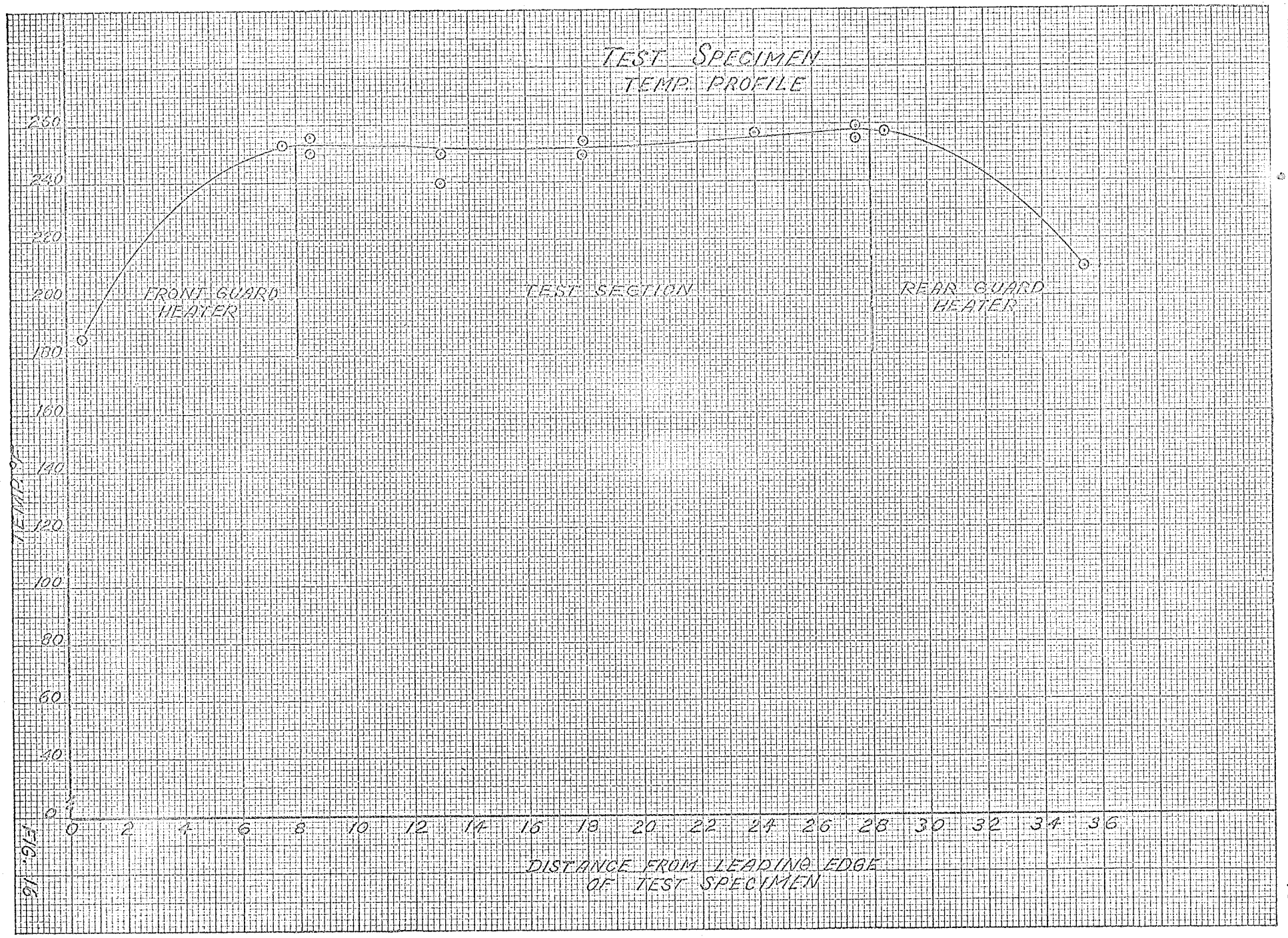

FIG. 16

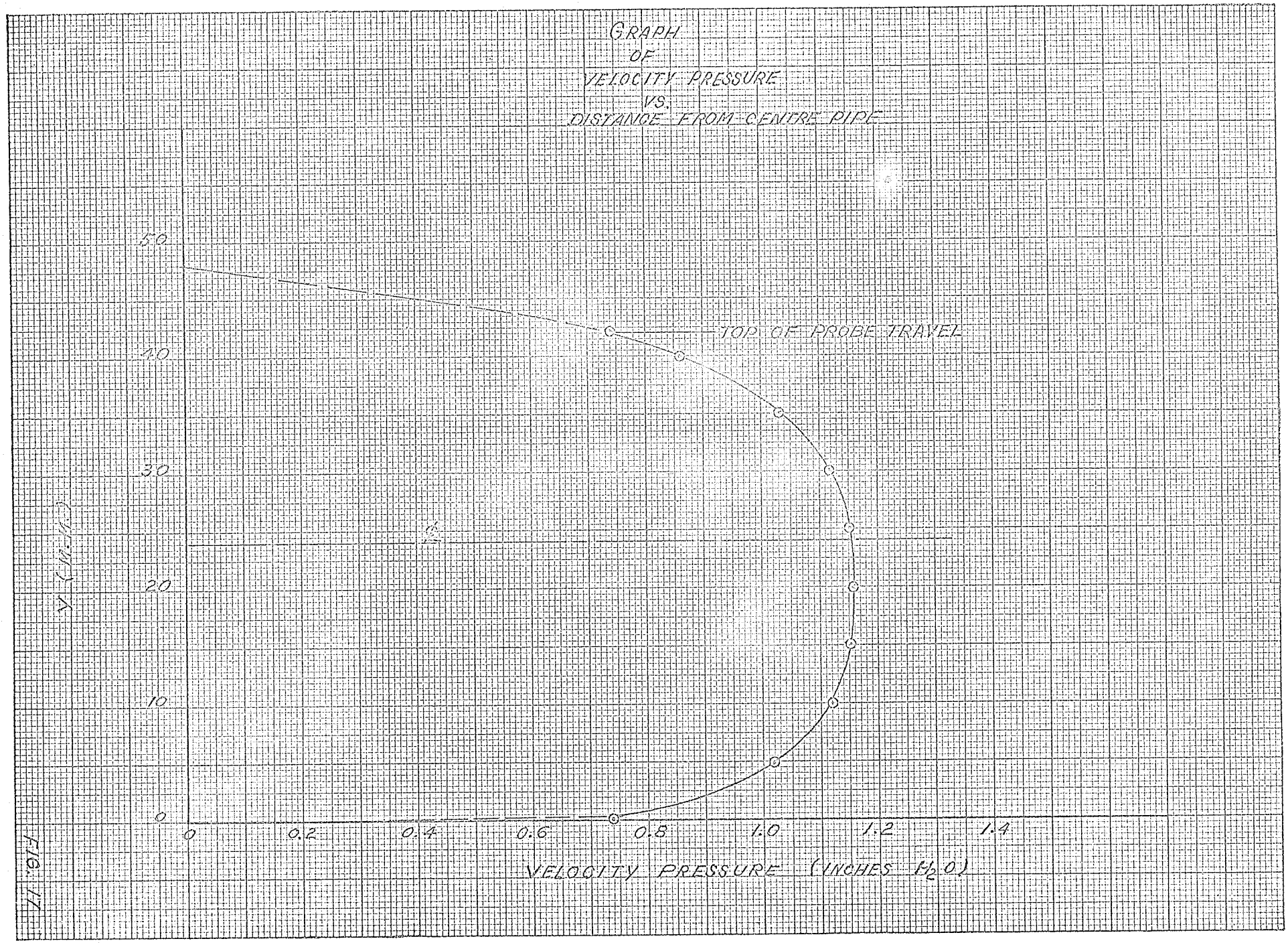

FIG. 17

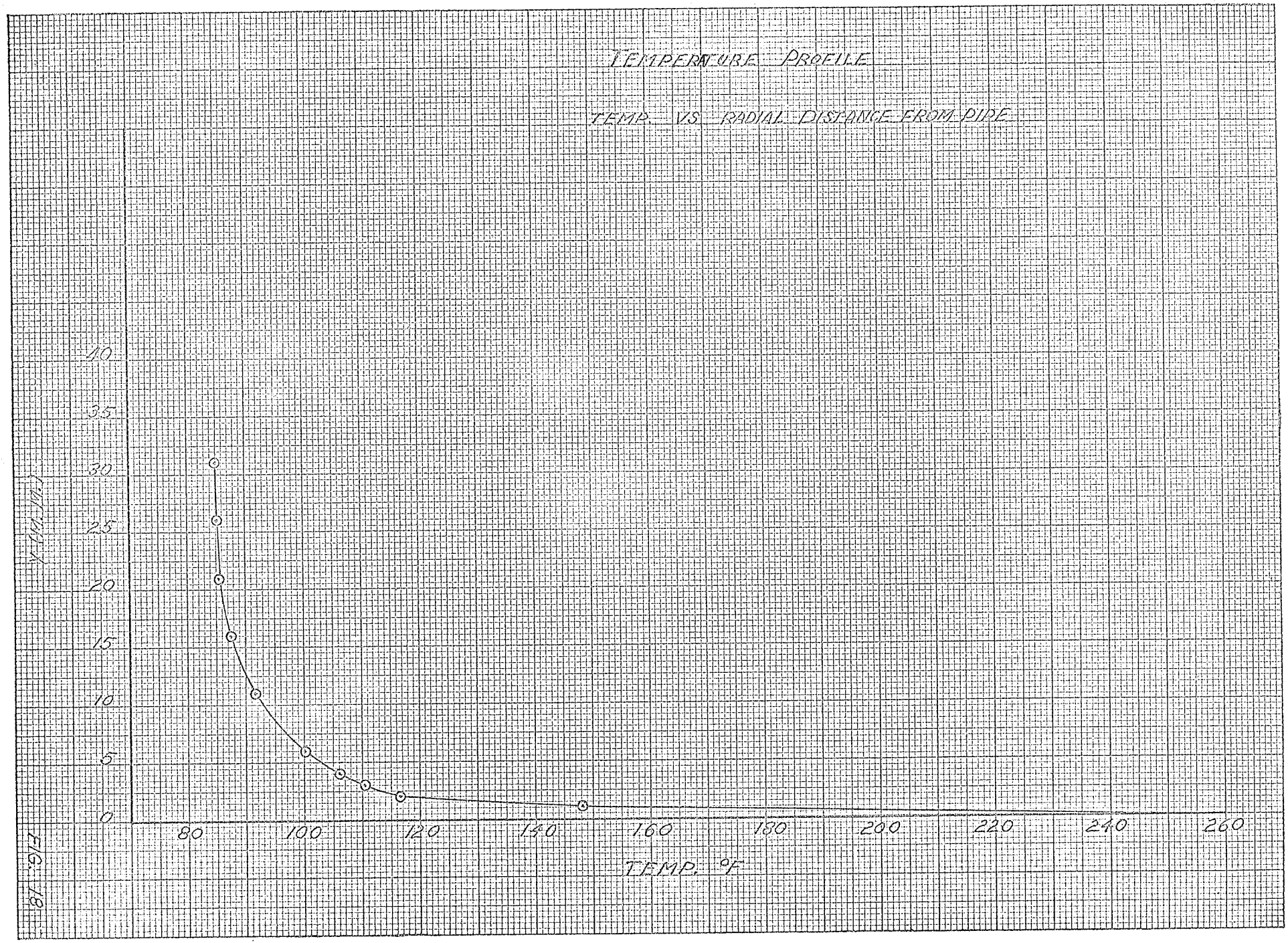

FIG. 18

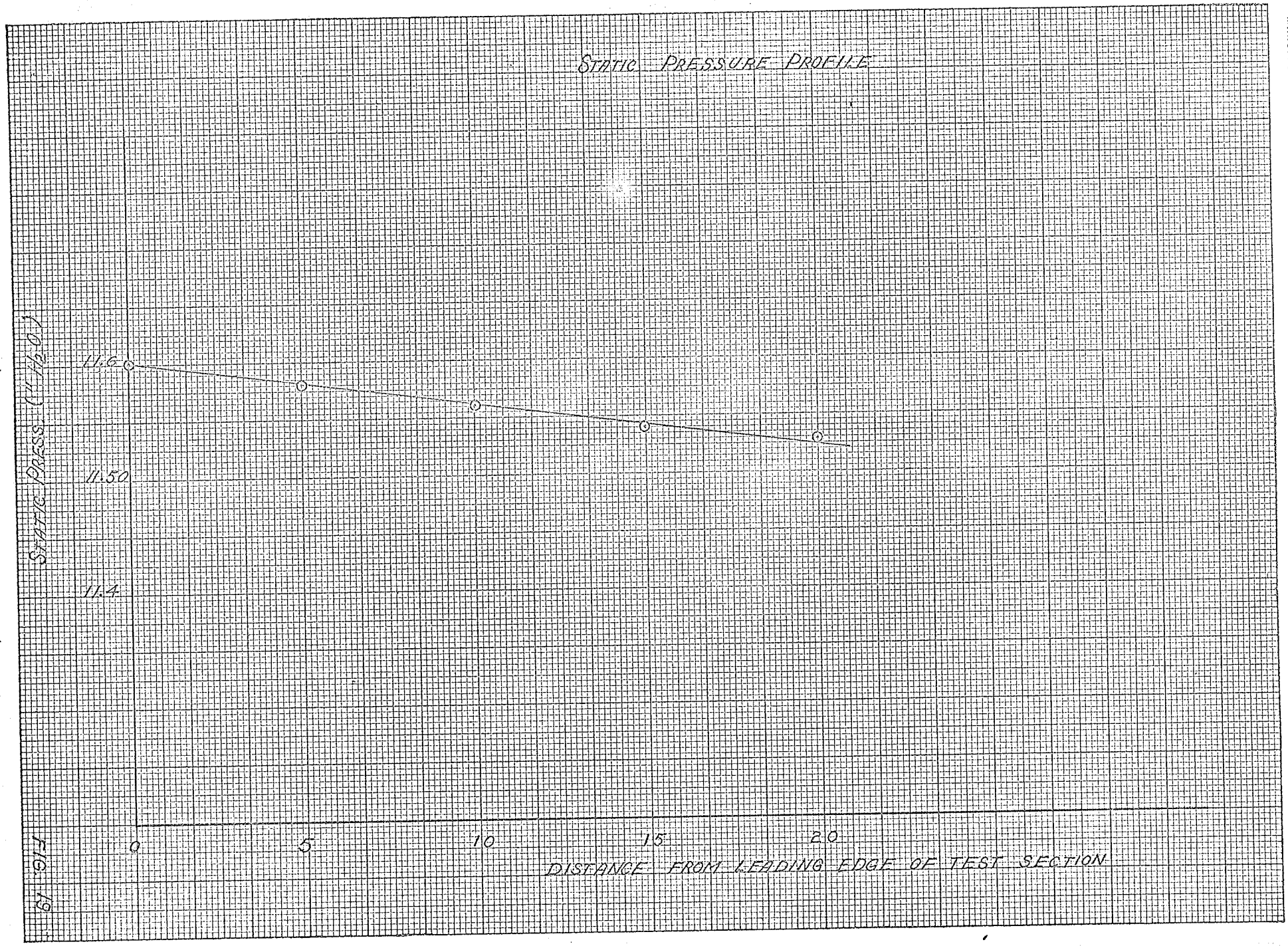

FIG. 19

CHAPTER 5

RESULTS AND CONCLUSIONS

In chapter two and three semi-empirical and some theoretical equations are stated. The following chapter is the comparison of these equations with the experimental results and the rating of the tubes on a heat transfer versus power consumption basis by Reynolds' analogy. The comparison of the experimental and published data is then followed by the conclusions that were drawn from these tests.

5.1 EXPERIMENTAL RESULTS

Referring to figure 16 the temperature profile over the complete test section was as predicted. The rise in temperature towards the downstream end of the section was due to the drop in temperature between the air and the test specimen causing a reduced heat transfer rate. The temperature rise of the test specimen was considered small enough to be neglected and the mean of the thermocouple readings was considered the mean temperature of the test section.

Figure 17 represents a typical velocity pressure profile obtained in the annular section. As predicted the maximum velocity did not occur at the centerline but was offset towards the inner pipe, approximately 4 millimeters, in the

profile shown. This offset varied from tube to tube but the basic shape of the profile remained constant. The temperature profile shown in figure 18 is similar in shape to curves in the published material for heat transfer from a surface to a fluid. Figure 19 is a curve of the static pressure taken from the inclined manometer the uniform slope being expected since there was nothing in the annulus to cause discontinuities.

The general shape of the kinetic energy and enthalpy profiles is shown in figures 20 and 21. The kinetic energy curves were drawn to zero from the lowest point taken in the profile since the $(\frac{u}{u_\delta})$ term in the product drops to zero while the other two ratios approach one. The same was true of the enthalpy profiles although not quite so noticable. By referring to figures 17 and 18 the curves approach zero at approximately the same rate with the temperature ratio being dominant until the $\frac{u}{u_\delta}$ ratio becomes small enough to cause the reversal of the curve.

The increase in area enclosed by the kinetic energy profile was relatively small as the distance increased from the leading edge of the test section while the enthalpy growth was considerably larger as can be seen by comparing the change in the areas enclosed by this curve. The hydrodynamic boundary layer was almost a constant thickness over the test section as

KINETIC ENERGY AND ENTHALPY PROFILES

KINETIC ENERGY

20 INCHES FROM LEADING EDGE

AREA = 4.31 SQ. IN.

$\left(\frac{u}{u_\delta}\right)\left(1-\left(\frac{u}{u_\delta}\right)^2\right)\left(\frac{R}{R_0}\right)$

15 INCHES FROM LEADING EDGE

AREA = 4.14 SQ. IN.

ENTHALPY

AREA = 1.43 SQ. IN.

$\left(\frac{u}{u_\delta}\right)\left(\frac{t-t_\delta}{t_w-t_\delta}\right)\left(\frac{R}{R_0}\right)$

AREA = 1.19 SQ. IN.

y (INCHES)

FIG. 20

Fig. 21

FORM 100

MANUFACTURED BY RENOUF PUBLISHING CO., MONTREAL

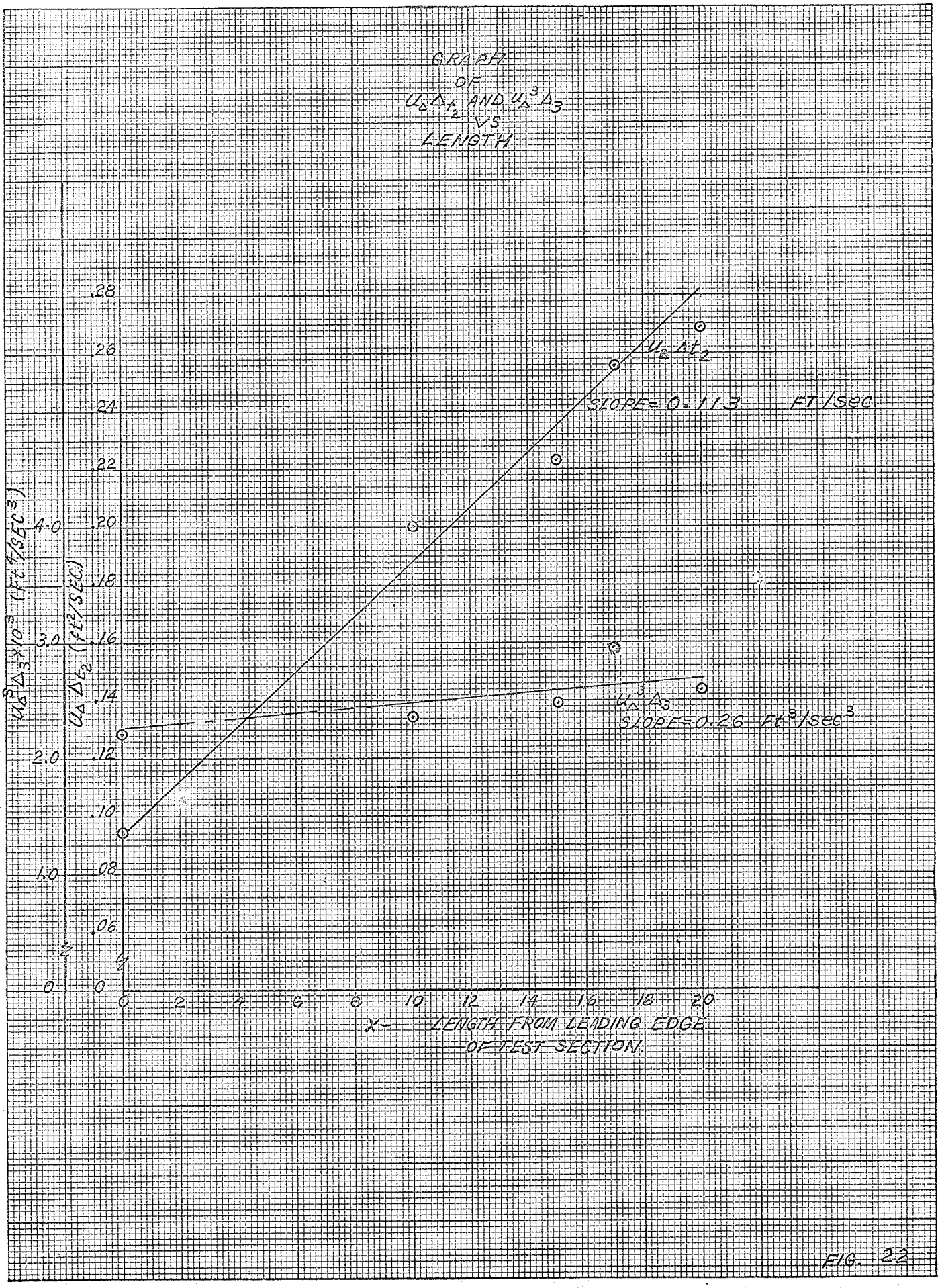

FIG. 22

can be seen by comparing the points of maximum pressure in table II of Appendix III. This relatively small change in the hydrodynamic boundary layer thickness accounts for the small changes in the kinetic energy thickness. Figure 32 of Appendix I shows the change in the thermal boundary layer over the test section, this accounts almost entirely for the change in enthalpy thickness along the tube.

The kinetic energy thicknesses were multiplied by u_δ^3 and enthalpy thicknesses by u_δ and curves similar to that shown in figure 22 were obtained. The small slope of the $u_\delta^3 \delta_3$ curve again emphasizes the relatively stable hydrodynamic boundary layer since large changes would be indicated due to the u_δ^3 term.

Figures 23,24,25 and 26 show the curves for the heat transfer coefficients obtained for each tube. The three heat transfer coefficients were calculated from the powerinput and the boundary layer profiles. The boundary layer profiles were used to calculate the local (L) and the average (M) coefficients from equations 3.13 and 3.18 respectively. It may be noted that the term "average coefficient" describes the coefficient that is applicable to the working length and is found by integrating the area under the curve of δ_{t_2} vs 'x'. The other value for the coefficient came directly from the heat balance. The values obtained from the heat balance were used for comparison with published data since they were considered

MACHINED SMOOTH TUBE

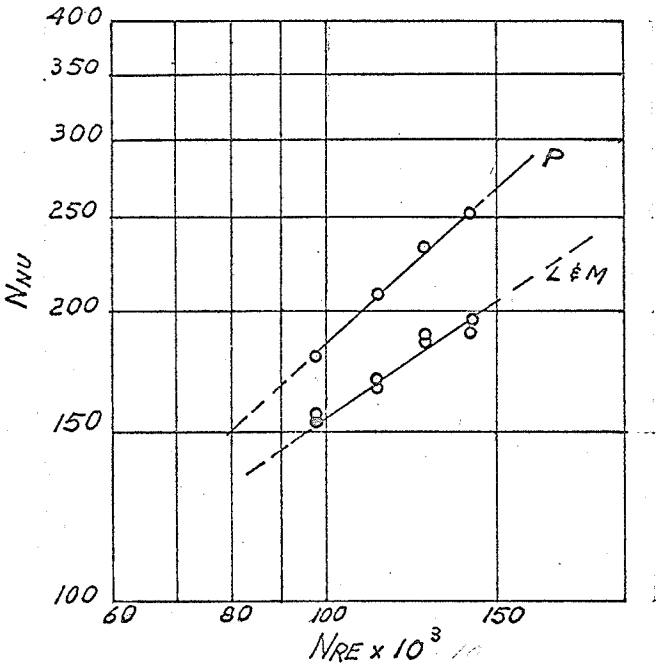

FIG. 23

SMOOTH STAINLESS STEEL TUBE

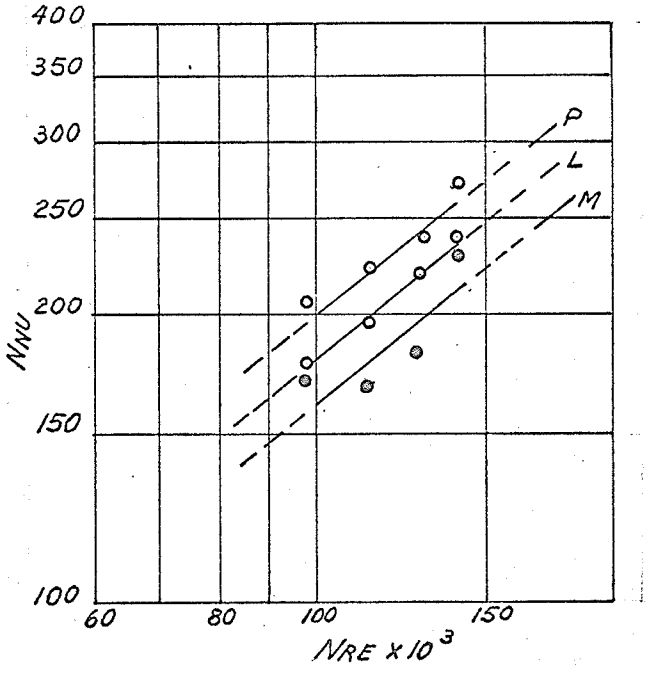

FIG. 24

P - HEAT BALANCE L - MEAN SLOPE OF Δt_2 VS 'X' (EQ'N 3-13)
M - AVERAGE h (EQ'N 3-18)

ROUGH STAINLESS STEEL TUBE

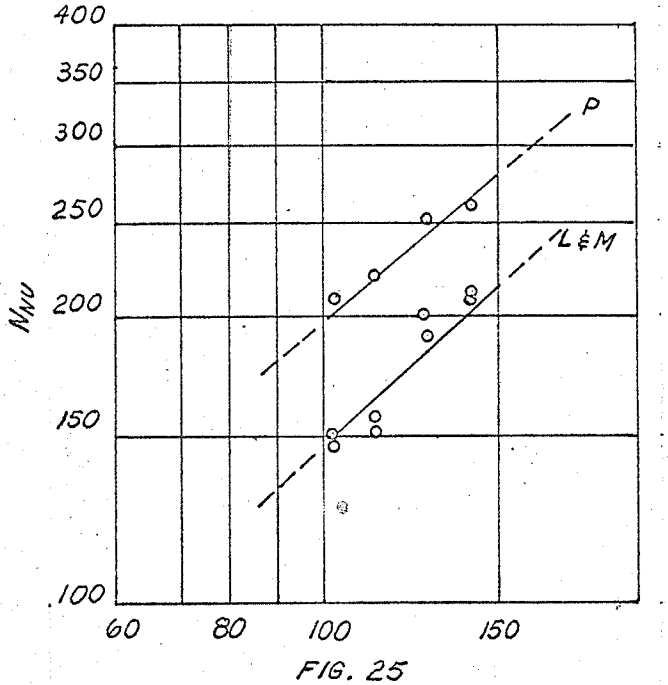

FIG. 25

KNURLED TUBE

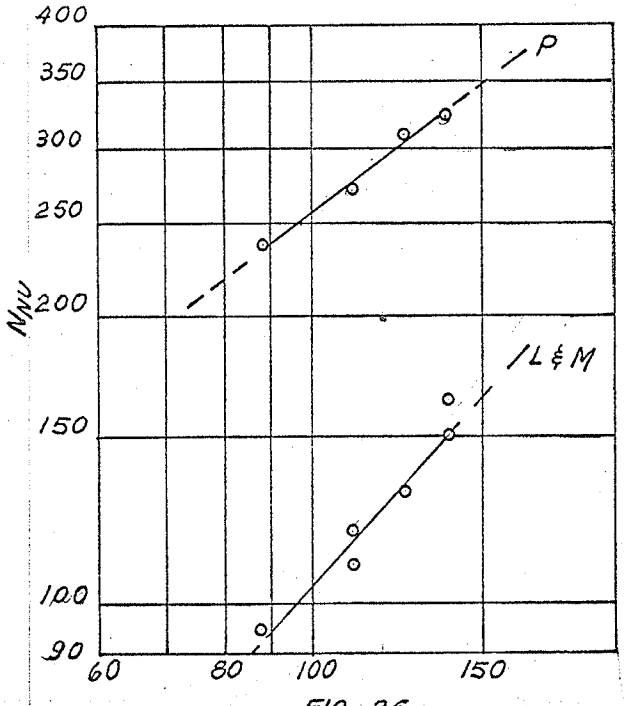

FIG. 26

the most accurate due to the smaller error in readings caused by measuring a larger temperature difference, and the overall accuracy of the heat balance as shown in Appendix I. Sample calculations of these three heat transfer coefficients are shown in Appendix III.

Figure 24 is the only graph where the two lines obtained from the boundary layer profiles did not coincide. Experimental error was suspected as the cause for the two low values of NNU evident for curve M in this figure. The tests represented by these values were run out of sequence. Although reproducibility was checked at frequent intervals these points were not re-run and an error in manometer readings of the profile probe would have accounted for the low values.

A close examination of figures 23 and 24 indicate that there was no measurable difference between the respective values of the Nusselt numbers. Therefore the contact resistance between the spray-welded stainless steel coating and the tube was negligible compared to deviations encountered in convective heat transfer data. Thus the inclusions in the bond between the coating and the tube as shown in the photographs had an insignificant effect on the heat transfer.

Figure 25 shows the values of NNU obtained for the stainless steel coated rough tube. Although there was some increase in heat transfer from this surface when compared with

the smooth tubes it was not significant. This indicates that the random roughness was not thick enough to penetrate the laminar sublayer and cause increased turbulence so that this height of roughness was ineffective.

For the knurled tube in figure 26 the two lines could have been brought closer together if the actual area of the knurled surface was used rather than the area obtained by using the mean diameter. The calculations for this surface area are shown in Appendix IV. The calculated knurled surface area was not exact although it was a good approximation. The fact that there appears to be an increase in the NNU (P) in figure 26 could have been partially due to this increase in area, since the Nusselt numbers calculated from the boundary layer profiles (L & M) indicate lower values. This seeming reduction in the heat transfer coefficients could be due to a thickening of the laminar sublayer caused by the fluid being held in place by this particular type of roughness. If the heat transfer coefficients were reduced the increase in surface area must have been large enough to offset this reduction and show a gain in the heat flow.

Figure 27 shows the friction factors that were obtained for each tube versus the NRE. The curves are all above those predicted by Barrow and McAdams for smooth tubes, but have essentially the same slope. There was some roughness on all

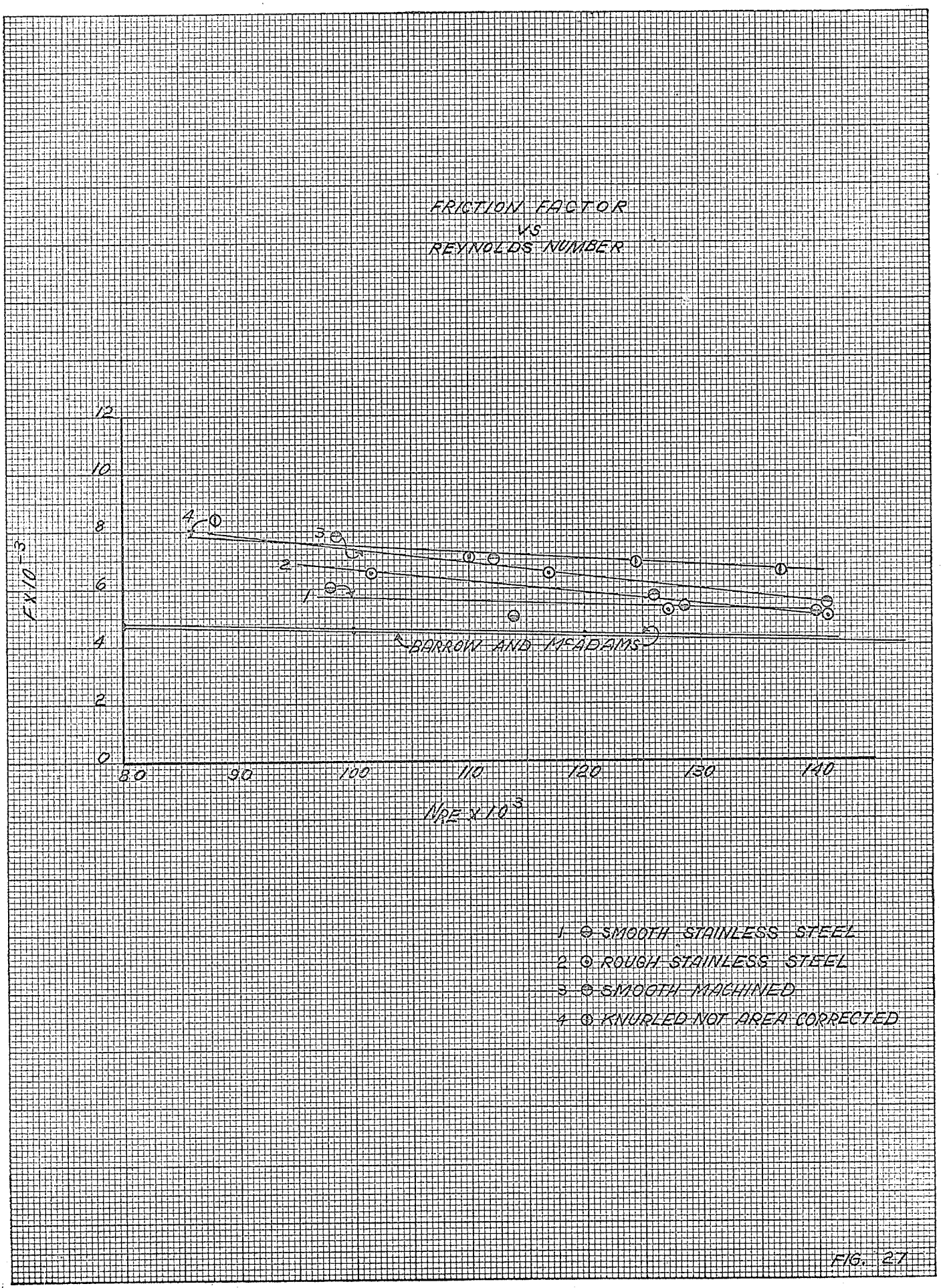

FIG. 27

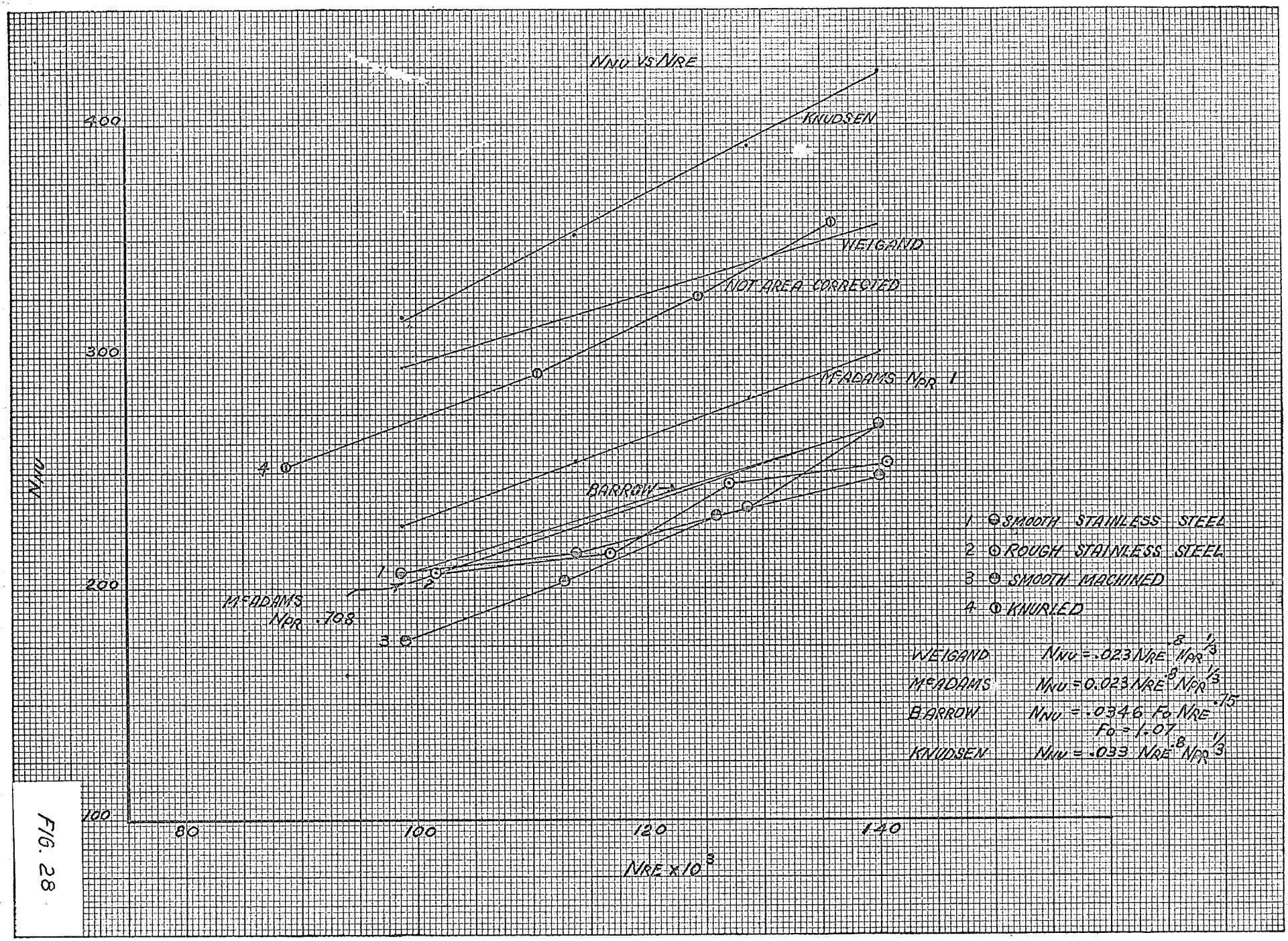

FIG. 28

the test sections which accounts to some extent for the higher values, with the knurled tube being highest.

Figure 28 gives a comparison of the results obtained in these tests and published data while figure 29 gives these same results but shows the relative roughness obtained for each tube. Barrow's equation is also shown on this graph with ± 25% limits on either side to show the agreement of the results with this formula. The slope of the experimental results is closer to McAdams 0.8 than the 0.75 predicted by Barrow's equation but well within the 25% limits. The results in this figure show an increase in heat transfer as the roughness increases. The rough and smooth metallized tubes do contradict this statement but they are very close together and experimental error could account for this disagreement.

Figure 30 is a comparison of Reynolds' analogy to the four tubes and Barrow's semi-empirical equation. This graph rates the tubes on a heat transfer versus power consumption basis, the lower the curve the greater the power consumption required for the same amount of heat transfer. It is generally conceded that an increase in heat transfer by roughening the surface is obtained at the expense of increasing the power consumption. However, if the curve for the knurled tube in figure 30 is considered it can be seen that increased heat transfer was obtained by very little increase in power consump-

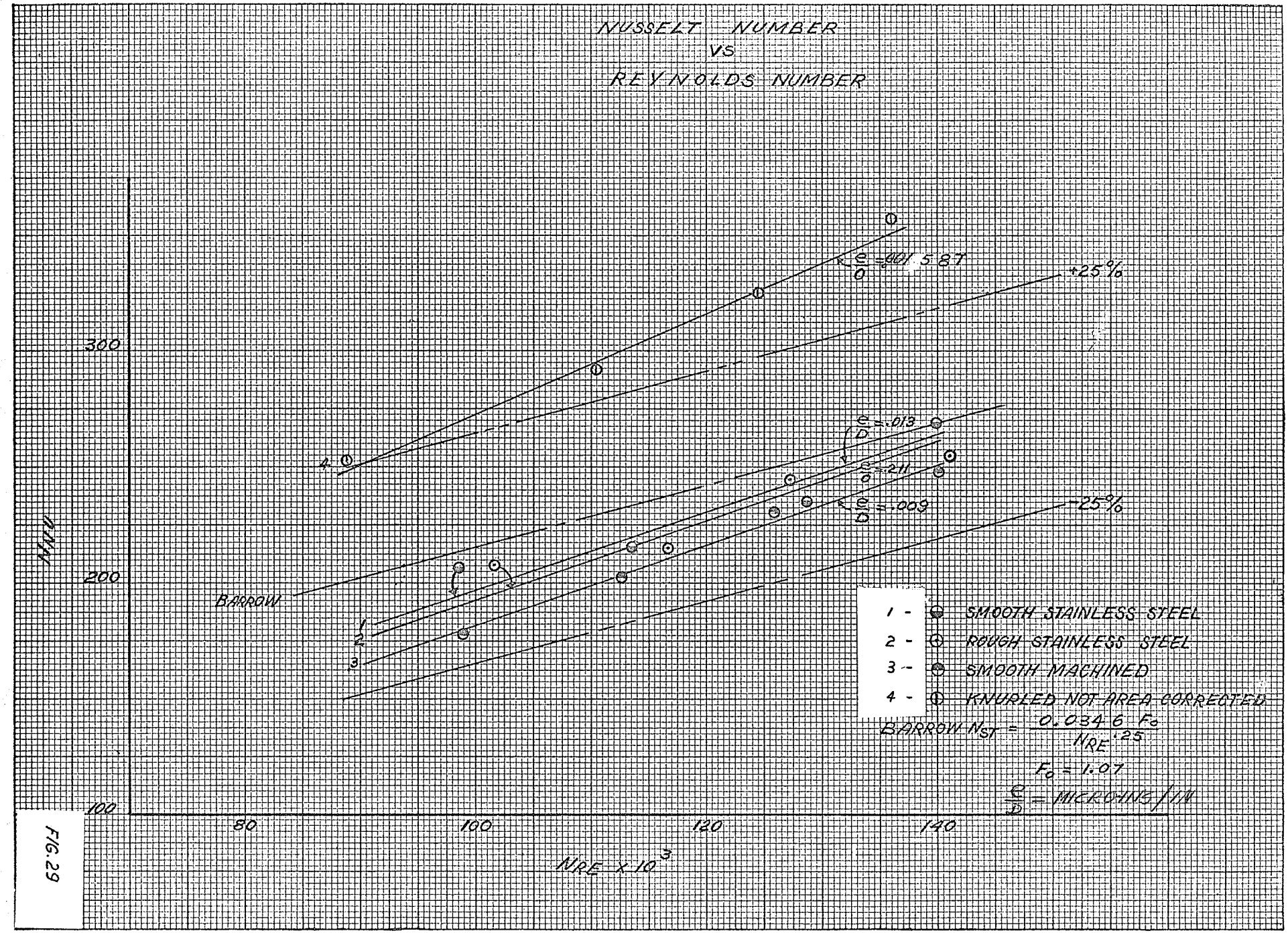

FIG. 29

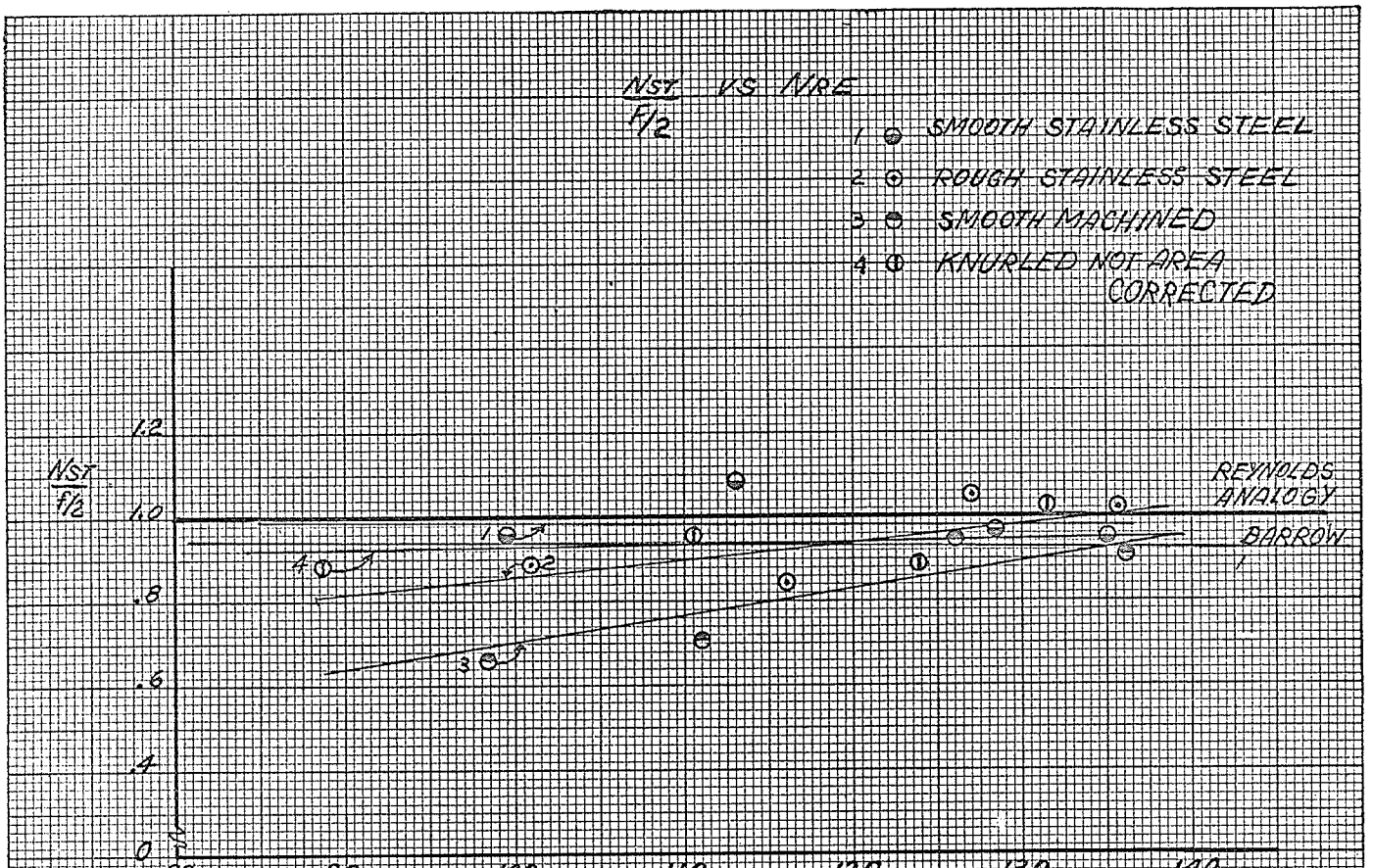

FIG. 30

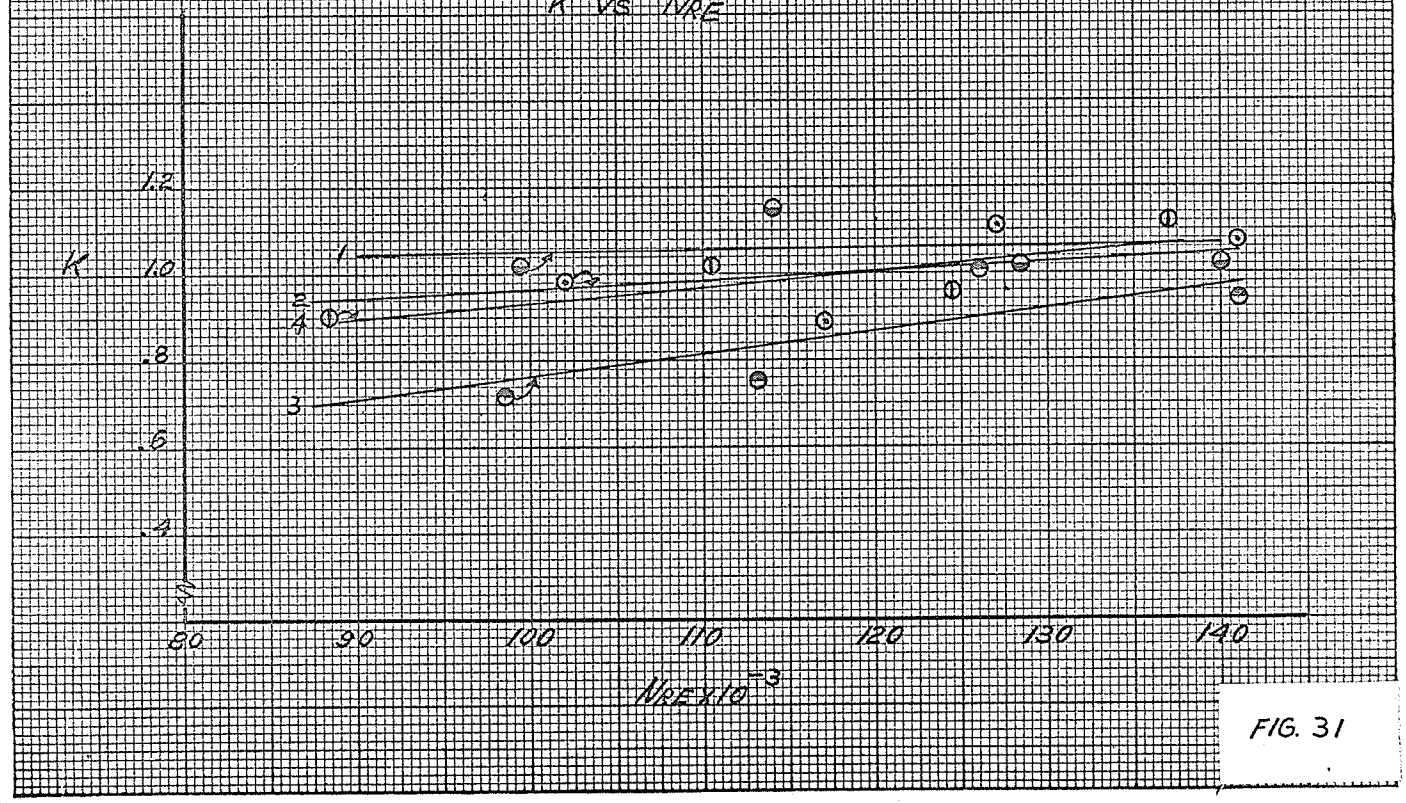

FIG. 31

tion so that the knurled tube is as effective a heat transfer surface as the smooth stainless steel tube. The smooth stainless steel and the knurled tube both very closely approximate Reynolds' analogy with slopes very close to Barrow's equation. The machined smooth and the rough stainless steel have a large deviation from the other two at the lowest Reynolds number but all are close at the upper limit. Again experimental error is the only reason which could account for this deviation particularly for the machined smooth tube.

Figure 31 shows the approximation of the tubes to Barrow's formula as taken from figure 30 and are given only as a comparison.

The results for the 350°F tests are not shown since there was very little variation of these with the values obtained at the 250°F test runs. The deviation between the heat transfer coefficients is shown in table I which was taken from a test on the knurled tube 20 inches from the leading edge of the test section.

TABLE I

COMPARISON OF 250°F AND 350°F TESTS

h	Temperature	
	250	350
Heat balance	8.28	7.83
Eqn. 3.13 Local	7.76	7.06
Eqn. 3.18 Avg.	7.17	7.17

5.2 CONCLUSIONS

The existing theory for the effect of roughness on the fluid friction and the heat transfer in an annulus has been reviewed and applicable equations developed from flat plate theory. It was found that this theory predicts the heat transfer coefficients for all but the knurled tube within 25%. The values for the knurled tube can be brought into line by applying an area correction calculated in Appendix IV. The values obtained by the boundary layer profile appear to be systematically low but a check of the theory and calculations produced no obvious error. The only assumption made in the theory that was of major concern was the neglecting of the heating effects caused by friction. There will be some heating but in the velocity range, which was from 50 to 80 ft. per second, no major error was inherent in this assumption.

This method of analysis does on the other hand give a greater insight into the effects of roughness on both the hydrodynamic and thermal boundary layers. The profile method could be used for a qualitative analysis of a heat transfer surface as to the effects of discontinuities of the surface on the boundary layers.

The relatively low roughness on the stainless steel tube had no apparent effects on the heat transfer rate either from the heat balance or profiles. This seems to indicate this

roughness did not disturb the hydrodynamic profile and that the laminar sublayer was thicker than the base to peak height of the roughness.

The knurled tube did have an effect on the boundary layers such that the heat transfer coefficients obtained from the profiles were reduced. For this to happen this type of roughness must have held the laminar sublayer in place and in fact thickened it.

The actual effects of the roughness height and shape on the laminar sublayer thickness could be better investigated by readings taken to within two or three thousands of an inch of the surface. The sublayer thickness for this Reynolds number range was in the order of 20 thousands of an inch and with this probe only measuring up to within 29 thousands this type reading could not be taken.

Finally,

1. Although the heat transfer coefficients obtained from the kinetic energy and enthalpy thicknesses are below those obtained from a heat balance they give a qualitative analysis of the effects of roughness on these coefficients.

2. A study should be carried out which investigates the hydrodynamic and thermal boundary layers very close to the heat transfer surface over a wider range of e/D. This

should be done with the possibility in mind of building up a family of curves for various values of e/D to be used to calculate heat transfer coefficients.

3. An investigation should also be carried out to determine the effects of the actual shape or type of the projections to evaluate air flow patterns around them.

A P P E N D I C E S

APPENDIX I

HEAT BALANCE CALCULATIONS

In order to calculate a heat balance the flow cross section was divided into eight equal areas as shown in the diagram below. This made the cross-sectional area equal to 3.11 square inches.

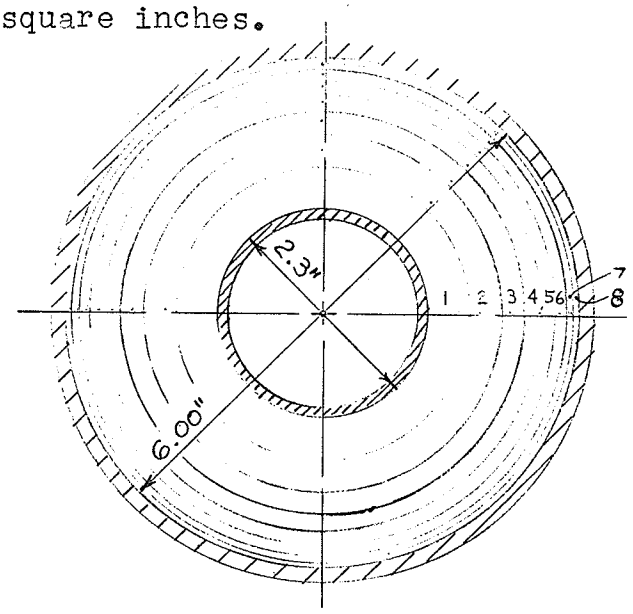

The average velocity and the temperature rise was found in each section by means of the velocity pressure and temperature profiles shown in figures 32 and 33.

In finding the temperature rise in these areas, particularly 1 and 2, the temperature was taken at the point where the cross-hatched areas in figure 32 are equal. These sample calculations were done for the knurled tube with uncorrected surface area.

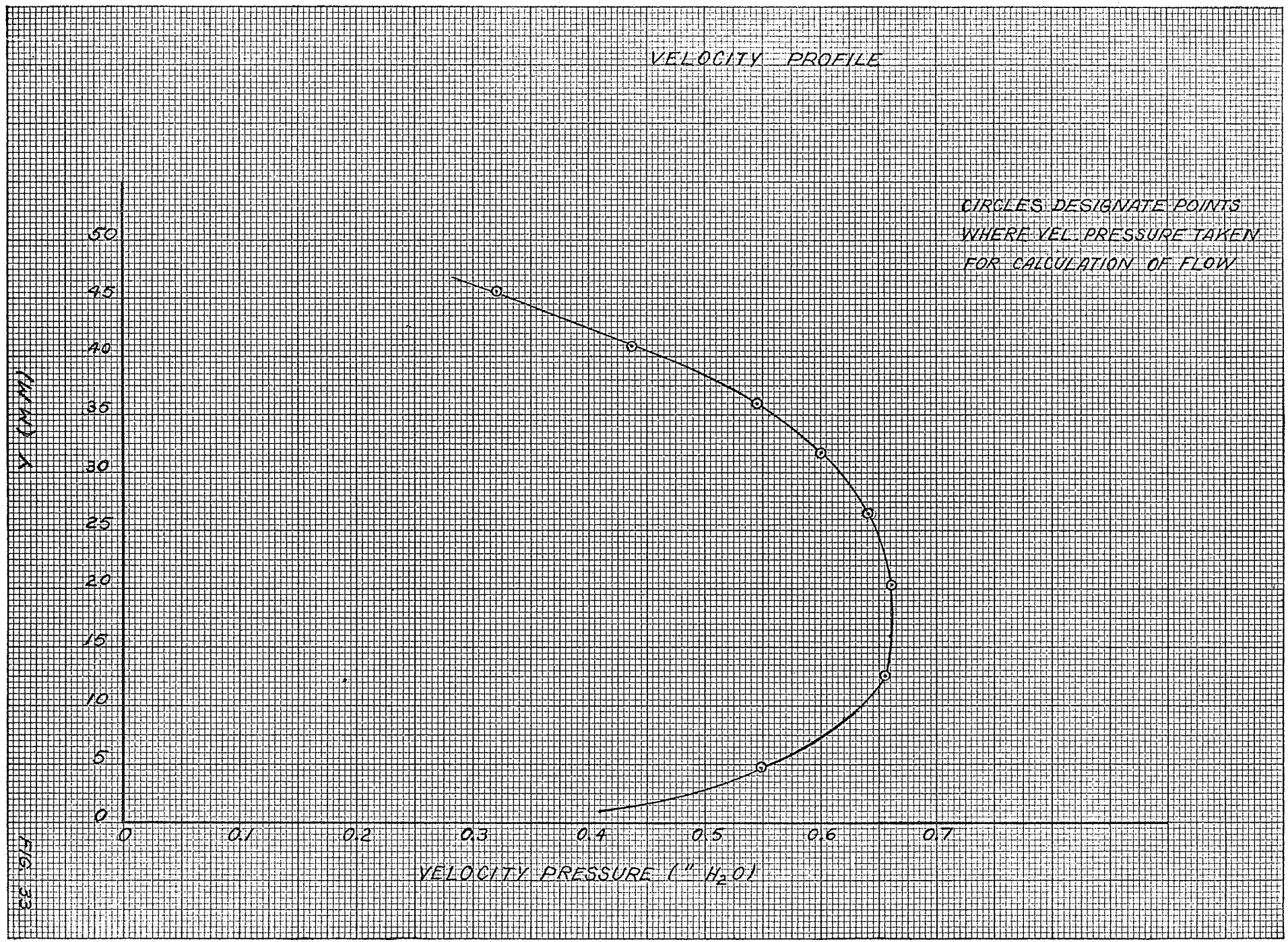

FIG. 33

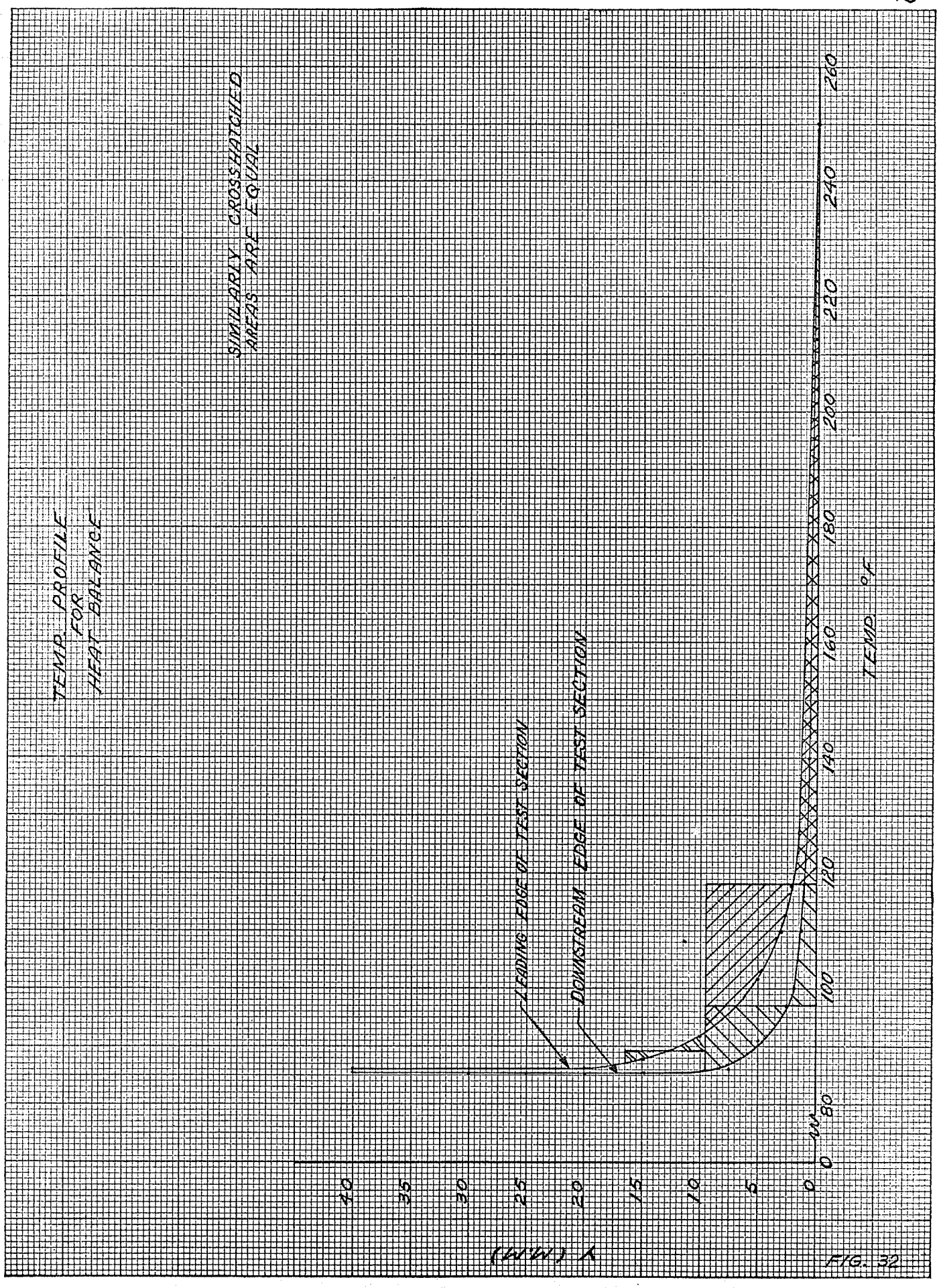

FIG. 32

Area 1.

Temperature = $102^{\circ}F$ = $562^{\circ}R$

Static Pressure = 1 " Hg.

Barometric Pressure = 29.33" Hg.

Total = 30.33" Hg. = 14.89 psia.

$$\text{Density} = \frac{14.89 \times 144}{53.3 \times 562} = 0.0716 \frac{\text{lbs}}{\text{cu.ft.}}$$

Velocity pressure = .545" H_2O

$$\text{Vel.} = 18.3\sqrt{\frac{h}{\rho}} = 18.3\sqrt{\frac{.545}{.0716}} = 2.76 \times 18.3 = 50.51 \frac{\text{ft}}{\text{sec.}}$$

Weight flow = ρ AU

$$= .0716 \times \frac{3.11}{144} \times 50.51 \times 3600$$

$$= 281 \frac{\text{lbs}}{\text{hr.}}$$

$$Q = Wc_p \Delta T$$

$$\Delta T = 18^{\circ}F.$$

$$Q = 281 \times 0.24 \times 18 = 1215 \frac{\text{Btu}}{\text{hr.}}$$

Area 2.

Weight Flow = 312 lbs/hr.

$\Delta T = 4^{\circ}F.$

$Q = 312 \times 0.24 \times 4 = 299$ Btu/hr.

Area 3.

Weight Flow = 314 lbs/hr.

Temperature Rise = $.5^{\circ}F$

$Q = 38$ Btu/hr.

Area 4.

$Q = 37$ Btu/hr

Area 5.

$Q = 36$ Btu/hr.

Area 6.

$Q = 34$ Btu/hr.

Area 7.

$Q = 31$ Btu/hr.

Area 8.

$Q = 26$ Btu/hr.

Total Heat to Air Flow = 1716 Btu/hr

Radiation Losses.

$$Q_R = \epsilon_1 \epsilon_2 \sigma F_{2-1} (T_2^4 - T_1^4)$$

ϵ_1 inside tube = 0.30

ϵ_2 outside tube = 0.74

E = emissivity

$\sigma = 0.1714 \times 10^{-8}$ $\frac{\text{Btu}}{\text{hr}\ ^\circ\text{F.}}$

$T_1 = 560^\circ R$

$T_2 = 710^\circ R$

$(T_2^4 - T_1^4) = 156.1 \times 10^8$

Assuming the outside surface as a black body and F_{2-1} equal to unity:

$$Q = 0.30 \times .1714 \times 156.1 = 80 \text{ Btu/hr-sq.ft.}$$

$$A = \frac{2.30 \times \pi \times 20}{144} = 1 \text{ sq.ft.}$$

$$\text{Total Heat Transfered} = 1716 + 80 = 1796 \quad \frac{\text{Btu}}{\text{hr.}}$$

$$= 528 \text{ watts.}$$

Power measured to Central Heater = 520 watts.

$$\text{Error} = \frac{8}{520} = 1.5\%$$

The 8 watts which constitute the error could originate with the assumption that the outside cylinder was a black body. The power metering equipment to the central heater was then assumed accurate enough for use in calculating the heat transfer coefficients.

APPENDIX II

CALCULATION OF FRICTION FACTOR FROM FANNING EQUATION

$$f = \frac{2g\rho\Delta P}{G^2} \left(\frac{De}{L} \right) \left(\frac{Di}{Do} \right)$$

These calculations are for test no.32 which was on the machined smooth pipe with a NRE = 98,300.

Δh on manometer = 0.09 inches.

Conversion factor for manometer = 0.725 in.H_2O/in.Man.

Δp over 20 inches, = 0.09x0.725x5.2=0.339 psf.

Static pressure = 0.85"Hg.

Barometric Pressure = 29.12" Hg

Absolute Press. inside section = 29.97"Hg. = 14.72 psia.

Mean flow temperature = 80°F. = 540°R.

$$\rho = \frac{14.72 \times 144}{53.3 \times 540} = 0.0737 \ \frac{\text{lbs}}{\text{cu.ft.}}$$

G from profile at outlet of 3 inch pipe.

Average velocity = average of $18.3\sqrt{\frac{h}{\rho}}$ = 183 ft/sec.

Outlet Temperature = 82°F

$$\text{Outlet density} = \frac{14.3 \times 144}{53.3 \times 542} = 0.0713 \ \frac{\text{lbs.}}{\text{cu.ft.}}$$

APPENDIX III

CALCULATION OF HEAT TRANSFER COEFFICIENTS AND DIMENSIONLESS NUMBERS

These calculations are for the same test as in Appendix II.

The temperature and pressure profiles were taken as shown in tables 2 and 3. Each profile was then analyzed and calculations completed to give tables 4,5,6,7 and 8. These results were then graphed as shown in figures 20 and 21. The area of each of these curves was measured with a planimeter with the areas as shown on the above figures. These areas must be multiplied by a scale factor of 0.04 $\frac{\text{in}}{\text{sq.in.}}$ to give the kinetic energy or enthalpy thicknesses. In the calculations the last term in equations 3.18 and 3.13 were neglected for the reason shown below.

From Eqn.3.18 the last term is:

$$\frac{u_\delta^{\,2}}{2\,C_p\,(t_w - t_\delta)} \qquad \frac{(\Delta 3L2 - \Delta 3L1)}{L_2 - L_1}$$

$C_p = 0.024$ Btu/lb ^oF.

$\rho_\delta = 0.0745$

$t_\delta = 1.198$ MV = 74^oF

$t_w = 6.471$ MV = 252^oF

TABLE II

VELOCITY PRESSURE PROFILES

HEIGHT FROM SURFACE (mm)	VEL. PRESSURE IN. H_2O	Distance From Leading Edge of Test Section (inches) 20	17	15	10	0
1		.27	.28	.295	.30	.35
2		.34	.34	.35	.36	.415
3		.375	.39	.395	.42	.46
4		.42	.43	.44	.46	.50
6		.48	.49	.50	.52	.565
11		.59	.60	.59	.62	.67
16		.66	.67	.66	.69	.73
21		.70	.72	.70	.72	.75
26		.71	.73	.705	.725	.76
31		.68	.70	.68	.70	.74

OUTLET VELOCITY PRESSURE PROFILE

Station	1	2	3	4	5	6	7	8	9	10	11
Pressure "H_2O	4.55	6.35	7.30	7.9	8.45	8.80	8.35	8.15	7.75	6.40	4.55

TABLE III

TEMPERATURE PROFILES

HEIGHT FROM SURFACE (mm)	THERMOCOUPLE READINGS (MILLIVOLTS)	Distance From Leading Edge of Test Section(inches) 20	17	15	10	0
1		3.160	2.855	2.825	2.745	2.868
2		2.190	2.262	2.222	2.122	1.852
3		2.043	2.096	2.071	1.961	1.698
4		1.902	1.959	1.939	1.840	1.578
6		1.718	1.782	1.785	1.669	1.442
11		1.443	1.490	1.482	1.433	1.328
16		1.291	1.368	1.362	1.343	1.309
21		1.228	1.303	1.312	1.311	1.309
26		1.198	1.282	1.299	1.300	1.309
31		1.194	1.282	1.299	1.308	1.309

Area ratio between annulus and 3 inch pipe.

Area 3 inch pipe = 0.0512 sq.ft.

Area of annulus = 0.173 sq.ft.

$$\text{ratio} = \frac{0.0512}{0.173} = 0.296$$

$$G = 183 \times 3600 \times 0.0713 \times 0.296 = 13{,}904 \ \frac{\text{lbs}}{\text{ft}^2 \text{ hr.}}$$

$$G^2 = \left(\frac{13{,}904}{3600}\right)^2 = 14.92 \ \frac{\text{lbs}^2}{\text{ft}^4 \text{sec}^2}$$

$$\frac{Di}{Do} = \frac{2.30}{6.09} = 0.383$$

$$\frac{De}{L} = \frac{6.09-2.30}{20} = 0.188$$

$$f = \frac{2 \times 32.2 \times 0.0737 \times 0.339 \times 0.383 \times 0.188}{14.92} = 0.0078$$

TABLE IV

DISTANCE FROM LEADING EDGE OF TEST SECTION = 20 INCHES

y (mm)	$\frac{u}{u_\delta}$	$\left(\frac{u}{u_\delta}\right)^2$	$1-\left(\frac{u}{u_\delta}\right)^2$	$\frac{R}{R_o}$	$\frac{u}{u_\delta}\left[1-\left(\frac{u}{u_\delta}\right)^2\right]\left(\frac{R}{R_o}\right)$	t	$t - t_\delta$	$\frac{t-t_\delta}{t_\rho-t_\delta}$	$\frac{u}{u_\delta}\left(\frac{t-t_\delta}{t_\rho-t_\delta}\right) \times \left(\frac{R}{R_o}\right)$
0	.617	.381	.62	1.025	.392	3.160	1.962	.372	.235
1	.692	.479	.52	1.062	.382	2.190	.992	.188	.138
2	.727	.528	.47	1.092	.373	2.043	.845	.160	.127
3	.769	.592	.41	1.126	.355	1.902	.704	.134	.116
5	.822	.676	.32	1.194	.314	1.718	.520	.099	.097
10	.912	.831	.17	1.363	.211	1.443	.245	.046	.057
15	.964	.930	.07	1.532	.103	1.291	.093	.018	.027
20	.993	.986	.01	1.701	.017	1.228	.030	.006	.010
25	1.000	1.000	.000	1.870	.000	1.198	.000	.000	.000

TABLE V

DISTANCE FROM LEADING EDGE OF TEST SECTION = 17 INCHES

0	.620	.384	.62	1.025	.394	2.855	1.573	.303	.193
1	.683	.466	.534	1.062	.387	2.262	.980	.189	.137
2	.731	.534	.466	1.092	.372	2.096	.814	.157	.125
3	.767	.589	.411	1.126	.355	1.959	.677	.130	.112
5	.819	.671	.329	1.194	.322	1.782	.500	.096	.094
10	.907	.822	.178	1.363	.220	1.490	.208	.040	.049
15	.958	.918	.082	1.532	.120	1.368	.086	.017	.025
20	.993	.986	.014	1.701	.024	1.303	.021	.004	.007
25	1.000	1.000	.000	1.870	.000	1.282	.000	.000	.000

CALCULATIONS FOR KINETIC ENERGY AND ENTHALPY PROFILE

TABLE VI

DISTANCE FROM LEADING EDGE OF TEST SECTION = 15 INCHES

y (mm)	$\frac{u}{u_\delta}$	$\left(\frac{u}{u_\delta}\right)^2$	$1-\left(\frac{u}{u_\delta}\right)^2$	$\frac{R}{R_o}$	$\frac{u}{u_\delta}\left[1-\left(\frac{u}{u_\delta}\right)^2\right]\left(\frac{R}{R_o}\right)$	t	$t-t_\delta$	$\frac{t-t_\delta}{t_p-t_\delta}$	$\frac{u}{u_\delta}\left(\frac{t-t_\delta}{t_p-t_\delta}\right)\times\left(\frac{R}{R_o}\right)$
0	.646	.418	.582	1.025	.385	2.825	1.526	.295	.195
1	.204	.496	.504	1.062	.377	2.222	.923	.178	.133
2	.748	.560	.440	1.092	.359	2.071	.772	.149	.122
3	.790	.624	.376	1.126	.334	1.939	.640	.123	.109
5	.842	.709	.791	1.194	.293	1.785	.486	.094	.095
10	.915	.837	.163	1.363	.203	1.482	.183	.035	.044
15	.968	.936	.064	1.532	.095	1.362	.063	.012	.018
20	.997	.993	.007	1.201	.012	1.312	.013	.003	.005
25	1.000	1.000	.000	1.870	.000	1.299	.000	.000	.000

TABLE VII

DISTANCE FROM LEADING EDGE OF TEST SECTION = 10 INCHES

0	.643	.414	.586	1.025	.386	2.745	1.445	.279	.184
1	.705	.497	.503	1.062	.377	2.122	.822	.159	.119
2	.761	.579	.421	1.092	.350	1.961	.661	.128	.106
3	.796	.634	.366	1.126	.328	1.840	.540	.104	.093
5	.847	.717	.283	1.194	.286	1.669	.369	.071	.072
10	.925	.855	.145	1.363	.183	1.433	.133	.026	.033
15	.976	.952	.048	1.532	.072	1.343	.043	.008	.012
20	.997	.993	.007	1.701	.012	1.311	.011	.002	.003
25	1.000	1.000	.000	1.870	.000	1.300	.000	.000	.000

TABLE VIII

DISTANCE FROM LEADING EDGE OF TEST SECTION = 0 INCHES

0	.685	.469	.531	1.025	.373	2.860	1.551	.300	.211
1	.747	.558	.442	1.062	.351	1.857	.548	.106	.084
2	.788	.620	.380	1.092	.327	1.695	.386	.075	.064
3	.820	.673	.327	1.126	.302	1.580	.271	.052	.048
5	.867	.752	.248	1.194	.257	1.446	.137	.027	.028
10	.944	.891	.109	1.363	.140	1.330	.021	.004	.005
15	.982	.964	.036	1.532	.054	1.312	.003	.001	.002
20	.997	.993	.007	1.701	.012	1.309	.000	.000	.000
25	1.000	1.000	0.000	1.870	.000	1.309	.000	.000	.000

$$u = \sqrt{\frac{2\rho\delta}{\rho\delta}} = 18.3\sqrt{\frac{h\delta}{\rho\delta}} = 18.3\sqrt{\frac{0.71}{0.0745}}$$

$$= 56.55 \frac{ft}{sec}$$

Δ_{3L2} = 4.31 x 0.04 inches = .1724 inches.

Δ_{3L1} = 3.39 x 0.04 inches = .1356 inches

Above term = $\frac{56.55x56.55x.0368}{2x0.24x178x778x32.2x20} = 2.75x10^{-6}$

First Term in eqn. 3.18.

$$\frac{\Delta_{t2L2} - \Delta_{t2L1}}{L_2 - L_1} =$$

Δ_{t2L2} = 1.43x0.04 = .0572

Δ_{t2L1} = 0.49x0.04 = .0196

Above term = $\frac{.0376}{20}$ = .00188 = $1.88x10^{-3}$

The last term was then considered of insufficient magnitude to be considered in the equation.

From 3.18 $NST_m = 1.88x10^{-3}$

$h_m = 1.88x10^{-3}x0.24x56.55x0.0745x3600$

$= 6.84 \frac{Btu}{hr.ft.^{\circ}F}$

Neglecting the last term in equation 3.13 and since the slope of the line in figure 22 was straight the local heat

transfer coefficient was constant.

slope = .113 $ft^2/sec.$

ρ_Δ = 0.0745 lbs/cu.ft.

Local h =.113x3600x0.0745x0.24= 7.27 $\frac{Btu}{hr.ft^2\ ^oF.}$

Taking the power input = 443 watts

surface area = $\frac{\pi x\ 2.3x20}{144}$ = 1 sq.ft.

T = 178 $^oF.$

$$h = \frac{443x3.412}{178} = \frac{8.64\ Btu}{hr.ft.^2\ ^oF}$$

Stanton Number.

$$NST = \frac{h}{C_p\ G} = \frac{8.64}{0.24x13,904} = 0.00259$$

With f from Appendix II

$$\frac{NST}{f/2} = \frac{0.00259}{0.0076/2} = 0.66$$

Nusselt Number. $= \frac{hDe}{k} = \frac{8.64x3.79}{12x\ 0.015} = 179$

Reynolds Number = $\frac{DeG}{\mu} = \frac{3.69x13,904}{3600x12x1.24x10^{-5}} = 98,300$

Prandtl Number = $\frac{\mu cp}{k}$ = 0.705
(from tables)

This process was repeated for each test.

APPENDIX IV

CALCULATION OF THE TRUE SURFACE AREA OF THE KNURLED TUBE

Analysis of the knurling.

PLAN VIEW

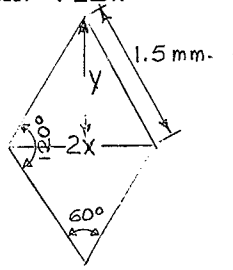

SIDE ELEVATION

Dimensions were made on a microscope with a magnification of 50 and a vernier scale on one lense

$1\frac{1}{2}$ m.m. = 0.059 inches.

Height = 0.007 inches

.059 inches = $\frac{1}{2}$ base length.

Length between large angles in plan view.

$$\frac{x}{0.059} = \sin 30^\circ = .5$$

$$x = 0.028 \text{ inches}$$

$$2x = 0.059 \text{ inches}$$

Area of $\frac{1}{2}$ base = 0.028 x 0.059 = 0.001652 sq.in.

Area of base = 0.003304 sq.in.

304 pyromids per square inch.

SURFACE AREA OF EACH DIAMOND

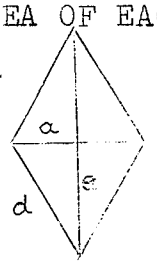

b = 0.007 inches
c = 0.028 inches

$$a = \sqrt{.b^2+c^2}$$

= 0.029 inches

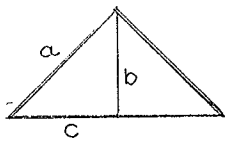

$e = \sqrt{a^2+d^2}$

$= 0.066$ inches.

Area of 1 face of pyramid = $\frac{1}{2}$ x 0.066x0.29 = 0.00096 sq.in.

Area of pyramid = 0.00384 sq.in.

Surface area per square inch of flat surface = 1.167 sq.inches.

ANALYSIS OF THREADS

18 threads per inch 0.014 inches wide
0.020 inches deep

Diameter = 2.29 inches

Area of lateral face of groove per revolution

= 0.20 x π x 2.29 x 2 = 0.29 sq.in.

Over length of tube = 0.29x18x20 = 104 sq.in.

Length left unthreaded = 1-(18x0.014)=0.75 $\frac{in}{in}$

Unthreaded surface = 15.0 inches

Smooth surface area = 108 sq.in.

Knurled = 108x1.167 = 126 sq.in.

Surface Area of Thread Base = 39 sq.in.

Total surface area = 104+126+39 = 269 sq.in.

Area of knurled and threaded tube = 1.87 sq.ft.

APPENDIX V

CALCULATION OF ARITHMETIC MEAN ROUGHNESS FOR KNURLED TUBE

Length of base 'y' from Appendix IV.

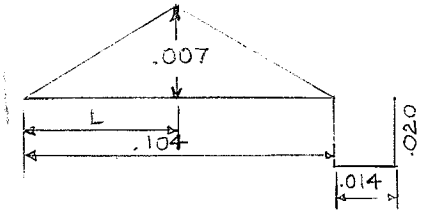

$$y = \sqrt{.059^2 - .028^2}$$

$$y = 0.052$$

$$2y = .104$$

Arithmetic mean roughness = e

$$e = \frac{1}{L} \int_0^L |y| \; dL$$

For $\frac{1}{2}$ of triangle $|y| = \frac{7}{52} \; LdL$

$$e = \frac{1}{52} \int_0^{52} \frac{7}{52} \; LdL$$

$$= \frac{7}{52^2} \left(\frac{L^2}{2} \right) \Big]_0^{52} = 3.5 \text{ thou.}$$

e for second half of triangle = 3.5 thou

$$e \text{ for threads} = \frac{10 \times 14}{14}$$

$$e \text{ for surface} = \frac{104 \times 3.5 + 10 \times 14}{118} = 4.270 \text{ milli-ins.}$$

$$\frac{e}{D} = \frac{4.270}{2.69} = 1587 \text{micro-ins/inch.}$$

BIBLIOGRAPHY

1. Barrow, H. A Semi-Theoretical Solution of Asymmetric Heat Transfer in Annular Flow. Journal of Mechanical Engineering, Vol.2. No.4, Oct. 1960.

2. Binder, R.C. Advanced Fluid Mechanics. Vol.II. Prentice-Hall Inc. 1958.

3. Brunello, G. Contribution A L'Étude de la Convection Forcée de la Chaleur sur des Parois Rugueuses. Publications Scientifiques et Techniques du Minitere de l'Air. 1958.

4. Carslaw, H.S., and Jaeger, J.C. Conduction of Heat in Solids Oxford at the Clarendon Press. 1959.

5. Chanda, B. Turbulent Boundary Layer Over Heated Plane Rough Surfaces. Thesis,Colorado State University, Fort Collins, Colorado, May 1958.

6. Croop, E.J., and Rothfus, R.R. Skin Friction Patterns for Transitional Flow in Annuli. AICHE Journal Vol.8, No.1.1962

7. Durant, W.S., and Mirshak, S. Roughening of Heat Transfer Surfaces as a Method of Increasing Heat Flux at Burnout. Pile Engineering Division A.E.C. July 1959.

8. Eckert, E.R.G., and Drake, R.M. Heat and Mass Transfer. McGraw-Hill Book Company, 1959.

9. Edwards, F.J., and Sheriff, N. The Heat Transfer and Friction Characteristics for Forced Convection Air Flow Over a Particular Type of Rough Surface. UKAEA. Copenhurst, Cheshire, England. 1961.

10. Kemeny, C.A., and Cyphers, J.A. Heat Transfer and Pressure Drop in an Annular Gap with Surface Spoilers. ASME Trans. Journal of Heat Transfer, May, 1961.

11. Knudsen, J.G. Note on j Factors for Turbulent Flow in Annuli. AICHE Journal. Sept. 1962, Vol.8. No.4.

12. Lancet, R.T. The Effect of Surface Roughness on the Convection Heat Transfer Coefficient for Fully Developed Turbulent Flow in Ducts with Uniform Heat Flux. ASME Heat Transfer Journal, May, 1959.

13. Levy, S., and Seban, R.A. Skin Friction and Heat Transfer for Laminar Boundary Layer Flow with Variable Properties and Variable Free Stem Velocity.ASME Paper No.53-SA-3. Mechanical Engineering, May, 1953.

14. McAdams, W.H. Heat Transmission. McGraw-Hill Book Company Inc. 1954.

15. McKay, J. Fluid Mechanics and Heat Transfer. Cambridge University Press.

16. Patterson, J., and Durands, K.J. Dimensionless Kinetic Energy: A New Parameter for Gas Flow in Ducts with Application to Nuclear-Power Reactors. Journal Mechanical Engineering Science, Vol.3. No.3. 1961.

17. Smith, J.W., and Epstein, N. Effect of Wall Roughness on Convective Heat Transfer in Commercial Pipes. AICHE Journal June 1957. Vol.3.No.2.

18. Nunner, W. "Wärmeübergang und Druchabfall in Rauhen Rohren" VDI Forschungsheft 455, 1956.